OSL DATING OF HIGH-ELEVATION ALLUVIAL SEDIMENTS: MCMURDO DRY VALLEYS, ANTARCTICA

A Thesis
Submitted to the Graduate Faculty
of the
North Dakota State University
of Agriculture and Applied Science

By

Meridith Ann Ramsey

In Partial Fulfillment of the Requirements
for the Degree of
MASTER OF SCIENCE

Major Program:
Environmental and Conservation Science

November 2014

Fargo, North Dakota

North Dakota State University
Graduate School

Title

OSL DATING OF HIGH-ELEVATION ALLUVIAL SEDIMENTS:

MCMURDO DRY VALLEYS, ANTARCTICA

By

Meridith Ann Ramsey

The Supervisory Committee certifies that this ***disquisition*** complies with North Dakota State University's regulations and meets the accepted standards for the degree of

MASTER OF SCIENCE

SUPERVISORY COMMITTEE:

Kenneth Lepper
Chair

Adam Lewis

Lisa Montplaisir

Approved:

04/16/2015
Date

Eakalak Khan
Department Chair

ABSTRACT

High-elevation alluvial fans in the McMurdo Dry Valleys are a record of short-term, occasional melting events along the margins of the East Antarctic Ice Sheet. Sediment samples were dated from five fans using Optically Stimulated Luminescence (OSL) dating. OSL dates the time since quartz grains were last exposed to sunlight; all sample preparation takes place in a dark room. Thirteen samples were dated for this thesis, the ages were stratigraphically consistent and ranged from 1.1 ka to 105.9 ka. Clusters of fan activity occurred between 1.1 and 3.1 ka and 8.1 and 11.1 ka. The melting events appear to be linked to insolation, with periods of fan activity occurring usually at times of increased mean annual insolation. The alluvial fans show promise as a possible archive for climate proxies in this region of Antarctica.

ACKNOWLEDGEMENTS

I would like to acknowledge the many people that helped make my time as a graduate student at North Dakota State University successful. I would like to thank my advisor Dr. Kenneth Lepper for his valuable assistance and advice. I would also like to thank my other committee members Dr. Adam Lewis and Dr. Lisa Montplaisir for their input throughout this process. I would like to thank Felix Zamora for his assistance in sample collection and with the many pit sketches and photographs throughout this thesis. Finally, I would like to thank my boyfriend and family for their constant encouragement.

DEDICATION

This thesis is dedicated to my mom, Paula Ramsey, and my grandmother, Carol Olson, for their constant encouragement and teaching me the importance of working hard and getting a good education.

TABLE OF CONTENTS

LIST OF TABLES

LIST OF FIGURES

CHAPTER 1. INTRODUCTION

The McMurdo Dry Valleys, located in the Transantarctic Mountains, of Antarctica, are in a polar desert that has been virtually unchanged for nearly 14 million years (Sugden et al., 1995). The Dry Valleys Region in southern Victoria Land is comprised of three ice-free valleys: Taylor, Wright and Victoria-McKelvey Valleys; making it the largest ice-free area in Antarctica. The area is ice-free because the Transantarctic Mountains block the flow of ice from the Polar Plateau into the area (Doran et al., 1999). The valleys, shown in Figure 1.1, are located between McMurdo Sound in the Ross Sea and the East Antarctic Ice Sheet. The area has a mean annual temperature in the valley bottoms of -14.8° to -30.0°C, and receives less than 100 mm of water equivalent precipitation yearly, making it an extremely arid polar desert (Doran et al., 2002). On the margins of the cold-based glaciers present throughout the valleys are streams flowing off the glaciers, depositing sediment, creating alluvial fans, lake deltas and lake-bottom deposits (Hambrey and Fitzsimmons, 2010).

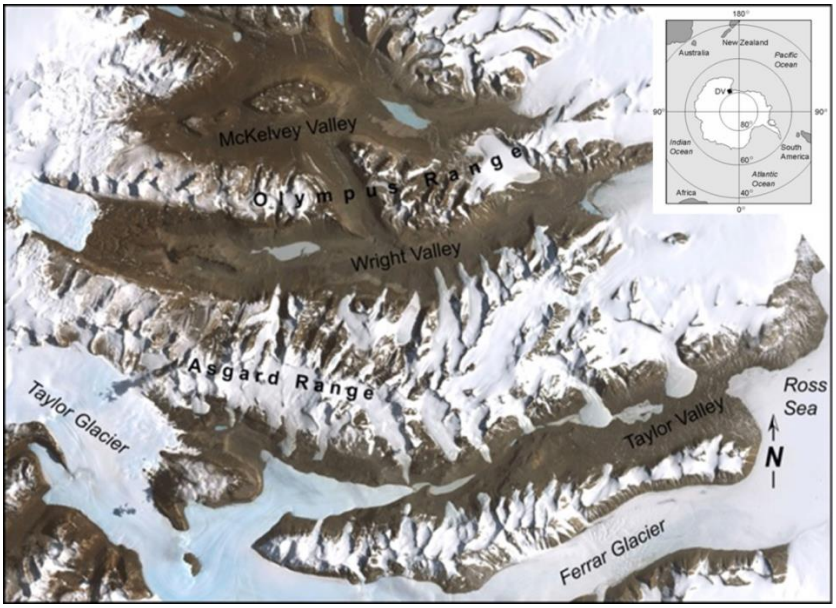

Figure 1.1. The Dry Valleys region of Antarctica. The three valleys are Victoria-McKelvey, Wright and Taylor. The Ross Sea is to the east, and the East Antarctic Ice Sheet is to the west. Base image courtesy of Polar Geospatial Center.

The Victoria-McKelvey Valley is the largest valley in the system, with an area of 650 km^2, running west to east for about 32 km (Kelly et al., 2002). In Figure 1.1, Victoria-McKelvey Valley is the uppermost valley shown. McKelvey Valley is located to the southwest of Victoria Valley, closer to Bull Pass. The valley floors range in elevation from 400 to 1000 m above sea level. Lower Victoria glacier stands between the valley mouth and the Ross Sea. The bedrock on the eastern end of the valley (closest to Ross Sea) is composed of granites, schist, gneisses and marbles, whereas the western end of the valley is composed primarily of sandstone with dolerite intrusions. Kelly et al. (2002) notes the north-central region of Victoria Valley has several large alluvial fans containing sand and gravel overlying the glacial till predominantly covering the valley floor.

Between McKelvey Valley and Wright Valley is the Olympus Range, with Bull Pass connecting the two larger valleys, as shown in Figure 1.1. Wright Valley is the middle valley of the Dry Valleys system. It is more than 50 km in length, extending from the polar plateau to the Ross Sea. The Wright Upper Glacier is located at the valley head and Wright Lower Glacier blocks the valley mouth. The floor elevations range from 85 to 300 m, and the walls have up to 1000 m of relief (Hall and Denton, 2005).

The third major valley in the Dry Valleys is Taylor Valley. Taylor Valley is 33 km long and about 12 km wide. It is bordered by the Asgard mountain range to the north, and the Kukri Hills run parallel to the Asgard range in the south, located in the southernmost portion of Figure 1.1. Taylor Glacier flows east from the Polar Plateau into the head of the valley (Nezat et al, 2001).

Small alluvial fans located at high elevations throughout the Dry Valleys are some of the youngest features on the landscape. The fans are located on Pliocene- to Miocene-aged tills. The

fans represent deposition associated with past meltwater generation. The melting events are inferred to represent a change from normal conditions in the Dry Valleys. Therefore, the fans could function as archives of melting events. The melting events, in turn, can function as a proxy for climate conditions along the East Antarctic Ice Sheet (EAIS).

Goals and Objectives

This thesis is part of an ongoing study of alluvial fans in the McMurdo Dry Valleys. The overall study is looking at the use of alluvial fans along glacial margins as an archive for climate change proxies in the Dry Valleys. A previous graduate thesis (Zamora, 2013) focused on the geomorphological and sedimentological aspects of the selected alluvial fans. He studied the fan sedimentology and stratigraphy to understand fan-forming depositional processes; and used geospatial analysis to study properties of the meltwater sources. This thesis will focus on the use of Optically Stimulated Luminescence (OSL) dating to determine when the alluvial fans have been active, and attempt to correlate the fan activity with available climate records to determine the extent and fidelity of climate proxy data recorded in alluvial fans.

The overall goal of this thesis is to build a timeline of marginal melting and fan building activity in the McMurdo Dry Valleys. This will be accomplished through the use of OSL dating. The first objective of this thesis is to address the unique complications related to the collection and processing of ice-cemented sediment samples for OSL dating. The alluvial fans are permanently ice-cemented beginning at a depth of 10-20 cm beneath the surface; collecting, storing and processing the ice-cemented sediment was a challenge for this project, as the samples could not be allowed to thaw, because mixing of exposed and unexposed sediment could have occurred. The second objective of this thesis is to generate a set of OSL ages for sediment deposition on several fans and from multiple sediment layers where possible. Deposition as

reflected in the OSL ages can then be used to constrain when the high elevation alluvial fans were active, and when melting may have occurred along the margins of the East Antarctic Ice Sheet. The third objective of this thesis is to attempt to correlate the OSL dates of fan activity to regional climate records and insolation models to determine the likelihood of melting occurring along the EAIS margin.

CHAPTER 2. LITERATURE REVIEW

General Concepts of OSL Dating

Optically Stimulated Luminescence dating, or OSL, is a dating method used to date the time since quartz or feldspar grains were last exposed to sunlight or heat (Wintle, 2008). OSL can determine time since a sedimentary feature formed or was altered (Lian and Roberts, 2006). It can work on samples of a wide variety of ages, from a few years to 120 ka, potentially including sediments as old as 300 ka (Bøtter-Jensen, 1997).

OSL has been in use since the mid-1980s, when it was discovered that the luminescence signal could be measured through stimulation by light in addition to heat (Wintle, 2008) as had been done previously in thermoluminescence (TL). OSL more closely simulates natural geologic processes than TL, because surficial sediments are exposed to light during transportation processes, whereas they are rarely exposed to the high levels of heat that TL replicates. There are a number of other benefits for using OSL versus TL. One benefit is that OSL utilizes the electron traps (storage sites) which are reset by light, which are more likely to be reset than the traps reset by heat, used for TL (Stokes, 1999).

The materials used for OSL dating are quartz and feldspar, two of the most common minerals on Earth. Quartz is used more commonly than feldspar because quartz has greater signal stability. In addition quartz does not respond to infrared stimulation as feldspars do, allowing samples to be tested for feldspar contamination. Quartz is formed in a variety of environments, for example igneous quartz crystallizes from a melt and metamorphic quartz can re-crystallize at a range of temperatures and pressures. The environments at the time of formation determine the chemical impurities and structural defects present in the crystal structure (Preusser et al., 2009). These imperfections act as traps for electrons that are produced when the

mineral grains are exposed to radiation from their surroundings (Lian and Roberts 2006; Bøtter-Jensen 1997). Free electrons are produced when the sediment is exposed to ionizing radiation, such as alpha and beta particles as well as gamma rays (Figure 2.1a). The radiation is emitted by the decay of radioactive elements in the mineral and the sediment around the mineral grains.

The electrons build up in the traps over time (Figure 2.1b), until the crystal is “saturated," when no more electrons can be stored (Stokes, 1999). When the grains are stimulated optically, or exposed to ionizing radiation, electrons are released from the traps (Fuchs and Owen, 2008) and can migrate within the crystal. Some of the electrons released may become re-trapped in a similar electron trap in the lattice with the remaining energy released as phonons, or released as a photon (Figure 2.1c). When the energy is released as a photon, the site (called a recombination center) is said to be excited, and it is from these sites that luminescence occurs (Preusser et al., 2009). This theory is called the energy band model and is discussed in detail in Preusser et al. (2009).

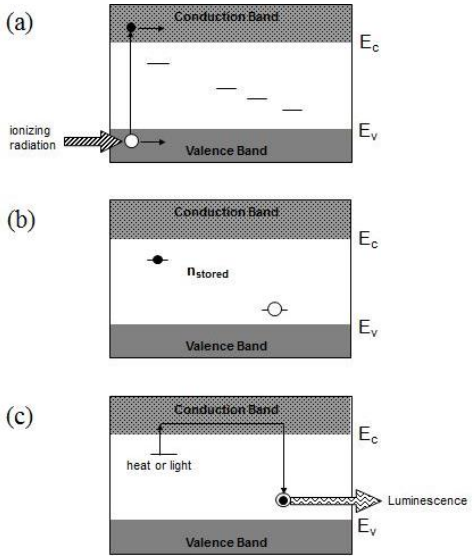

Figure 2.1. Simple model for stimulated luminescence in an insulator. **(a)** charge pair production by ionizing radiation **(b)** “trapped” charged localized at crystal defects **(c)** stimulation of trap site, release of charge, and radiative recombination (from Lepper, 2001).

Lian and Roberts (2006) discuss the various types of traps present in minerals that allow luminescence to occur. After recombination occurs, any excess energy is released as heat (lattice vibrations) or as luminescence (photons). Light can empty some of the electron traps; while, for others, light stimulation has no effect. Because exposure to sunlight is enough stimulation to begin the process of ejecting the electrons from traps, the samples are collected and processed in darkness or specially filtered light. Heat exposure can empty most traps. Some traps can hold electrons for only a few days while others can hold electrons for up to millions of years. It is these "deep traps" that are used for OSL dating. The electron traps and recombination centers in quartz are related to defects in the lattice. The defects can be due to silicon or oxygen vacancies, or substitutions in the structure, such as additional Al or Ti (Preusser et al., 2009). The photon emissions are detected by a photomultiplier, and recorded as an OSL decay curve (Preusser et al., 2009).

In order to calculate a date the dose absorbed in nature, the "equivalent dose" (D_e) must be determined by luminescence measurements. An additional portion of the sample is analyzed for concentrations of U, Th, K, Rb and their daughter products, from these concentrations an environmental "dose rate" (D') is calculated. The OSL age is calculated by dividing the equivalent dose by the dose rate (Lian and Roberts 2006; Duller 2008; Stokes 1999).

$$t_{OSL} = \frac{D_e}{D'} \qquad \text{Eqn. 2.1}$$

Where t_{OSL} is the OSL age in years, D_e is the equivalent dose absorbed by the sample expressed in J $kg^{-1}$and D' is the environmental dose rate expressed a J kg^{-1} yr^{-1}.

The most common procedure used for finding the D_e for quartz samples is through the single aliquot regenerative protocol (SAR; Figure 2.2). The SAR protocol consists of a series of cycles to make a calibration curve for every subsample of the field sample. The first cycle is a measure of the radiation dose the sample received in nature. The next cycles consist of the aliquot being exposed to increasing amounts of laboratory radiation (Duller, 2008). The sensitivity of the sample is tested during each cycle by the application of a fixed dose, and the response for these test doses can be plotted to determine if changes in the sensitivity occurred.

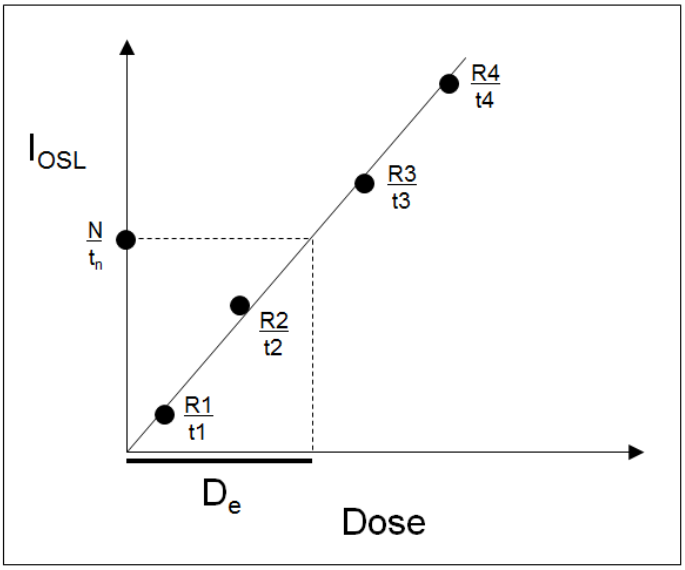

Figure 2.2. Graphical representation of equivalent dose determination by single-aliquot regenerative dose (SAR) techniques. Note that the data points are the "test dose normalized" ratios and the D_e is found by interpolation (from Lepper, 2001).

Review of specific studies using OSL dating in Antarctica

OSL is a more useful dating method than more commonly used methods, such as radiocarbon dating, in the Dry Valleys because radiocarbon requires the presence of organic carbon material in the sediments, which is uncommon or even non-existent in the area (Fuchs

and Owen, 2008). Radiocarbon dating is also limited in the age to which it can date due to the short half-life of ^{14}C; it can only work for samples less than 50,000 years old.

Using OSL in Antarctica has some unique challenges that are not typically encountered using this process in other parts of the world. The difficulties in Antarctica come from its geographic location, OSL related issues such as low-signal intensity and difficulty distinguishing samples with insufficient bleaching, have been encountered by many of the other researchers attempting to use OSL in Antarctica (Berger and Doran, 2001; Bristow et al., 2010). Optical dating has not been used extensively in Antarctica. It has been used mostly along the coast of East Antarctica, in a number of freshwater lakes where the lacustrine sediments have been dated to infer the timing and extent of past glaciations. Dating those sediments with radiocarbon was difficult because of the lack of radiocarbon and the very old ages of the sediments, as well as complications from upwelling of old sea water (Fuchs and Owen, 2008).

Fuchs and Owen (2008) note that luminescence dating could be a very useful tool in Antarctica, although insufficient bleaching is a problem in the environments they have studied that needs to be addressed. Insufficient bleaching occurs when the sediments do not receive enough sunlight exposure for the electron traps to be completely emptied prior to burial (Stokes, 1999; Rittenour, 2008). In sediments that have been transported by water, this is especially likely to be an issue due to the turbidity of water with a high sediment load (Rittenour, 2008). It is necessary to ensure that sufficient bleaching has occurred. This can be determined by examining the distribution of equivalent doses determined from numerous aliquots of the field sample (Lepper et al., 2000; Lepper and McKeever, 2002), checking the age estimate against the stratigraphy to see if it is a reasonable age, or comparing the OSL age with a different dating method, such as radiocarbon (Fuchs and Lang, 2009; Rittenour, 2008).

OSL dating in the McMurdo Dry Valleys

Within the Dry Valleys region, OSL and TL have been used to correct age estimates from radiocarbon in lacustrine sediments. As part of the ongoing study of Lake Hoare, depositional ages of lake-bottom sediments were compared using a number of dating methods, including TL, radiocarbon, and paleomagnetism (Doran et al., 1999). The paper addressed benefits and problems with each of the methods used. The results were compared to determine which methods were the most accurate for use in the Dry Valleys. Doran et al. (1999) notes that IR-OSL would be the preferable method to use for dating Dry Valley sediments; the use of radiocarbon was problematic because of difficulties understanding the carbon reservoir effect in Antarctica. Berger and Doran (2001) completed tests to see how effective daylight was at zeroing sediment for TL and IRSL dating of sediment from various depositional environments in the Dry Valleys. IRSL is a luminescence dating method where feldspar grains are stimulated by near infrared wavelengths of light (Sohbati et al., 2012). Sediment had problems with being incompletely zeroed in this study (Berger and Doran, 2001).

Berger et al. (2010a) expanded on previous papers (Berger and Doran 2001; Doran et al., 1999) using luminescence dating methods in Lake Hoare, in Taylor Valley. The lake bottom sediments of the lakes in the Dry Valleys are records of lake level history as well as containing evidence of microbial life in the lakes. The methods for determining sediment deposition rates included radiocarbon, multigrain TL and OSL and single-grain OSL (Berger et al., 2010a). OSL dating provided a more realistic age estimate of the bottom deposits than radiocarbon. The sediment-transport conditions at Lake Hoare appeared to be sufficient for zeroing of silt and sand grains to occur.

Multiple perched deltas, from times of much higher lake levels, around Lake Fryxell in Taylor Valley have been dated using OSL to establish a lake level history. The paleodeltas are from glacial Lake Washburn, which is estimated to be up to 40 times larger than the current lake size (Hall et al., 2000). Previously, lake level history has been determined using ^{14}C dating of lake cores and deltas (Hall and Denton 2000; Hendy and Hall, 2006). Radiocarbon results for the lake cores have been problematic, because there is a large ^{14}C reservoir affect on the bottom of the lake due to the permanent ice cover and salinity stratification (Berger et al., 2013; Doran et al., 1999). The deltas consist of algal mats along with beds of sand and silt. The sand and silt were dated using OSL. The results were stratigraphically consistent and several thousand years younger than the algal mats previously dated using radiocarbon (Berger et al., 2013; Hall and Denton, 2000). Modern sediments, recently deposited, gave an average age of 90 ± 20 a, indicating that the quartz sediments were effectively zeroed before deposition.

OSL was used to date dunes and determine the dune migration rates in the Packard dune field along the northern margin of lower Victoria Valley, near Lake Vida (Bristow et al., 2010). Sediment transport by wind is one of the few types of sediment transport actively occurring in the area. The dunes migrate at a slow rate due to the bimodal wind patterns in the area and being frozen much of the time. OSL has been used to constrain the ages of the dunes and calculate dune migration rates. The sediment was not frozen at the time of sampling. Bristow et al. (2010) found that the quartz used in the study had very low OSL intensities, and displayed signs of incomplete zeroing before deposition. However, OSL experimental and analytical methods exist to compensate for these signal properties. Overall, the dunes had good OSL date results for the phases of dune migration (Bristow et al., 2010).

OSL dating on the Antarctic Peninsula

Sediment traps were deployed in Andvord Bay and Brialmont Cove at the Antarctic Peninsula for a year to collect sediment (Berger et al., 2010b). The sediment was tested to see whether effective zeroing of sediment was occurring for TL and OSL methods to be applied. A sediment trap is a series of funnels anchored into the lower water column, sediment in the water column becomes trapped in the funnels, as illustrated in the sediment trap configuration used for luminescence dating shown in Figure 2.3 below (Berger et al., 2009; Berger et al., 2010b). Berger and his fellow researchers found that the sediment collected from the lower traps had almost no exposure to daylight for zeroing to occur, the top trap had some light exposure. In their interpretation TL and single-aliquot OSL had poor results, with large age overestimations, and wouldn't be good techniques to use for dating the bottom sediments according to Berger et al. (2010b).

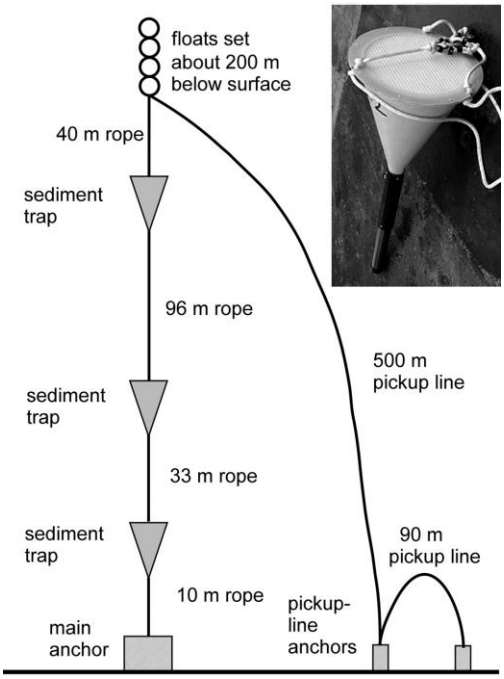

Figure 2.3. A sediment trap configuration. The suspended sediment in the water is collected in the series of funnels. Image from (Berger et al., 2009).

OSL dating has been used on Alexander Island, by the Antarctic Peninsula, on raised epishelf lake deltas and former subglacial Hodgson Lake. The water levels in the epishelf lakes are controlled by a hydraulic connection to the sea, the paleodeltas were dated to determine past sea level changes (Roberts et al., 2009). The sediment in the samples was exposed to enough sunlight to ensure sufficient bleaching; however, there wasn't enough quartz present in most of the samples to allow dating. The dates that were obtained were used to create a Relative Sea Level Curve (RSL), which could be compared with RSL curves from other locations around the Antarctic Peninsula to determine sea level history for the area (Roberts et al., 2009).

OSL dating in the remainder of Antarctica

One of the first uses of infrared stimulated luminescence dating (IRSL) in Antarctica was by Krause et al. (1997) in the Schirmacher Oasis, in East Antarctica. IRSL is similar to OSL, except feldspar is used and instead of being stimulated with light in visible wavelenghts, the electrons are stimulated using near-infrared light (Sohbati et al., 2012). Coarse plagioclase feldspar grains were used to test if the short transport distance into the lake was enough daylight exposure for resetting to occur. Plagioclase was used due to a lack of preferred quartz and alkali feldspars. No anomalous fading was detected with the plagioclase (Krause et al., 1997). Anomalous fading occurs when charge is lost over time from theoretically stable traps; it can lead to an age underestimation (Spooner, 1994).

Multiple studies in Antarctica have developed the use of beach cobbles for OSL dating, as a means of determining sea level history. Simms et al. (2011) used optical luminescence to reconstruct sea levels on the South Shetland Islands in Antarctica. They dated quartz grains from the undersides of cobbles found in elevated beaches left from times of past high sea levels. The age estimates were consistent with each other, and using the same technique on a modern beach

produced an age of zero, suggesting that the techniques used were an effective and useful way to date beach sediments around the world (Simms et al., 2011). The dates obtained using OSL in this study were also consistent with radiocarbon dates obtained from the same sites. The main challenge faced by Simms et al. (2011) was the lack of quartz for dating as the beach cobbles were mainly mafic igneous rocks without quartz crystals.

OSL dating in other permafrost regions

Going to the opposite end of the Earth, OSL has been used to date perennially frozen sediments in Siberia (Arnold and Roberts, 2011; Arnold et al., 2008). Arnold and Roberts (2011) focused on what the effects of being frozen might be on sediments used for OSL. The samples collected by Arnold et al. (2008) were frozen and collected using a drill with a coring bit. Despite the low light signals, frozen sediments were found to be good candidates for OSL dating. They found that sediments coming from frozen deposits had lower light intensities than other sediments did, but that may have been attributed to the original source of the quartz than as a result of being frozen (Arnold and Roberts, 2011). The samples' ages were stratigraphically consistent and matched other dating methods (Arnold et al., 2008). Arnold's three papers about OSL in Siberia (Arnold et al., 2008; Arnold and Roberts, 2011; Arnold et al., 2011) all show OSL to be a reliable method for dating sediments in a permafrost environment.

Alluvial Fans-Morphology & Effects of Climate

Alluvial fans have a semi-conical form, as a result of sediment-filled flows entering the lowland area through a point then becoming unconfined and spreading out laterally at the fan apex (Blair and McPherson, 1994; Bull, 1977; Stock et al., 2008). The fan apex is the point where the source channel intersects the mountain front at the tip of the fan. When the sediment is primarily carried by water, it is called an alluvial fan (Stock, et al. 2008). Alluvial fans occur in

areas of unconfined streamflow. Sediment deposition occurs when the stream is unable to transport the sediment through the accumulation area due to the decrease in stream confinement or due to an increase of sediment load being supplied to the stream (Bull, 1977). The sediment is spread radially from the center, with the edges being thinner than the middle (Blair and McPherson, 1994).

The primary processes that transport sediment to the alluvial fans are debris flows, sheet floods, rock falls and rock avalanches (Blair and McPherson, 1994; Parker, 1999; Crosta and Frattini, 2004). The two most important processes for building alluvial fans are debris flows and sheet floods. Their influence can vary based on tectonic or climatic controls and spatial variations in the depositional processes (Bull, 1977; Wells and Harvey, 1987).

The most common process contributing to the building of an alluvial fan is sheet flooding, an occasional unconfined water flow that expands laterally as it moves downslope. Sheet floods develop when a flash flood reaches the fan and spreads out due to the lack of channel walls and the multidirectional slope of the fan surface (Blair and McPherson, 1994). This occurs frequently after excessive rainfall or rapid snowmelt. Sheet flows cover a large amount of the fan during a single event (Parker, 1999).

Debris flows are also a significant source of sediment on many alluvial fans. A debris flow is a mixture of sedimentary particles and a small amount of water and air moving downslope due to gravity. Blair and McPherson (1994) write that the main mechanism leading to debris flows on alluvial fans is the transformation of a colluvial slide into a debris flow through the introduction of water and air to the sediment as it moves downslope. In general, fans formed primarily through debris flows have a steeper gradient than a fan formed through sheet flooding (Stock et al., 2008; Wells and Harvey 1987).

Alluvial Fan Morphology

The morphology of an alluvial fan is controlled by several factors including the slope angle, lithology of the sediment, water and sediment discharge, and the climatic and tectonic environment (Bull, 1977). The depositional slope of the fan is gradual, from 1.5 to 25°. The sediment and water discharge are both influenced by climate and the grain size distribution of the sediment.

Grain size in an alluvial fan can range from silt and clay-sized to gravel and boulders (De Chant et al., 1999). Fans usually have planar bedded deposits, with deposits growing more fine-grained downfan. Gravel is deposited in the upper part of the fan, sand further out, and silt sized particles on the far edges of the fan (Stock et al. 2008). Because of the short transport distance of sediment and low amounts of reworking, alluvial deposits are often poorly sorted and angular. Sheet floods are recorded in the sediment through planar-bedded deposits with a dip of 2° to 8°, parallel to the fan surface (Blair and McPherson, 1994). The stratigraphic sequence of fans is a record of short term events (in the case of the Dry Valley fans, the events are melting), with sufaces in between representing normal conditions (the desert pavement surfaces present in some of the profiles in this study).

Flows on an alluvial fan are generally unconfined. As sediment accumulates on the fan, the channels may shift as deposition raises the surface of part of the fan, deposition may shift to a lower portion (Bull, 1977). Steep slopes along the higher portions of the fan often contain large amounts of sediment that can be remobilized and redeposited on the fan. Sediment is often moved through catastrophic events such as rapid snowmelt or heavy rainfall and flash flood type events that don't occur frequently. Water movement in fan channels is relatively rare and infrequent; sediment movement on a fan is through a combination of water flow and mass-

wasting (Blair and McPherson, 1994). Fans are built up over time by the deposition point moving laterally, seeking the lowest topography (Parker, 1999).

Fan morphology is a result of tectonics and climate. Tectonics influence fans by contributing to high sediment supplies and influencing fan gradients. When mountains are being uplifted, the steepness of the fan slope may increase, which in turn changes the structure of the fan (Harvey et al., 1999). Tectonically influenced fans are commonly thicker than fans influenced primarily by climate and the areal extent of tectonically influenced fans is controlled by the sediment supply (Bull, 1977). The morphology of the large alluvial fans on the Ganga plain in India are controlled tectonically, while the sediment supply to those fans are controlled by the climate (Goswami and Mishra, 2013). Fans are influenced by climate through changes in the volume of water and sediment provided to them. Fans around the world accumulate sediment more quickly during wetter conditions.

Alluvial Fans and Climate

Alluvial fans may be found in all types of environments, but generally are more common in arid climates. Periods of increased deposition indicate either periods of increased sediment yields or periods of decreased competence of transport modes, both of which are related to the influence of climate on alluvial fans (Bill, 1977). Fans have been successfully used previously as an indicator of past climate change, with fans recording increased temperature or precipitation in the past. In the southwestern United States, alluvial fans were used to study the historical effects of the El Niño Southern Oscillation (ENSO) climate pattern (Bacon, et al., 2010). The ENSO climatic pattern leads to wetter winters in the desert southwest, which is reflected by increased flooding, landslides and channel erosion in the fan sediment record. Bacon, et al. (2010) correlated the sediment records of alluvial fans with climate proxies available in the American

southwest to test the effectiveness of alluvial fans as a climate proxy in the region. Alluvial fans in the Atacama Desert, a hyper-arid desert in Chile, are also activated on El Niño timescales. Low-magnitude precipitation events were sufficient to activate the fans and modify the fan surface (Haug, et al., 2010).

In addition to the well studied arid region alluvial fans, fans are also found in paraglacial areas. Paraglacial features are landforms, land systems and landscapes directly influenced by former glaciation and deglaciation (Ballantyne, 2002). Ryder (1971) writes about the unique features of paraglacial alluvial fans in British Columbia and compares the fans to those in the American Southwest. The paraglacial fans are composed of glacially-derived sediments reworked by fluvial or mass wasting processes, and only active for a short time following deglaciation (Ryder, 1971).

In polar regions, Snow melt, and the melting of glaciers and permafrost are the water sources for polar alluvial fans. Fans in these regions are only active for a few months of the year (Lønne and Nemec, 2004). In the Canadian Arctic, alluvial fans in permafrost regions are dominated by sediment gravity flows and gelifluction, as well as processes related to annual snowmelt (Catto, 1993). Although the fan in Catto's 1993 study was not directly influenced by alpine glaciers, its growth appears to have been more rapid under glacial cimatic conditions. The fan has continued to develop at a slower rate during drier post-glacial conditions.

Review of specific research applying OSL to alluvial fans and footslope deposits

Many studies related to the dating of alluvial deposits and colluvium have used OSL as a dating method. Incomplete bleaching is a common problem when using OSL to date these sediments. In perfect conditions, OSL signals can be completely bleached with just a few seconds of light exposure. However, colluvial and alluvial deposits rarely have those perfect

conditions; instead the sediment is in turbid water or movement occurs in primarily gravity driven events (Fuchs and Lang, 2009). This reduces the likeliness that the sediments will receive enough light for the signal to be completely reset. As a result, being able to detect insufficient bleaching is necessary when dating sediments optically.

A large number of alluvial fans have been studied using OSL dating in the American southwest (DeLong and Arnold, 2007; Sohn et al., 2007; Stock et al., 2008). In southern Death Valley, OSL has been used to determine if climate or tectonics had a bigger effect on alluvial fan activity (Sohn et al., 2007). The ages obtained by Sohn et al. (2007) shows that alluvial fans were building during periods when the climate transitioned from wetter to drier and during cool periods.

Stock et al. (2008) used OSL as part of a larger study of fan morphology to determine the active dates of four alluvial fans in the American southwest. They collected samples from the widest active channel and the base of the deepest bank exposure. The dates they found were consistent with dates from other methods (radiocarbon and U-Th dating) used on the same fans (Stock et al., 2008). Delong and Arnold (2007) used radiocarbon, OSL and cosmogenic radionuclide dating in the western Transverse Ranges of California to date alluvial fans and determine the accuracy of each dating method in that setting. The OSL results were stratigraphically consistent and were similar to the results from the other dating methods; OSL appeared to be a better choice due to an abundance of suitable material (quartz) being available (DeLong and Arnold, 2007).

Two studies have used OSL dating on alluvial fans in the Andes Mountains of Argentina. One study used OSL to date alluvial deposits in intramontaine basins of northwestern Argentina. The study looked at the effectiveness of OSL on various facies (Robinson et al.,

2005) and the climatic significance of the results (Spencer and Robinson, 2008). They found that facies associated with alluvial fans are suitable for OSL dating, with partial bleaching (the signal not being completely reset) not a problem in the study area. A second study in Argentina used luminescence dating to determine the geologic history of several large alluvial fans underlying a city (Schmidt et al., 2012). The fans had been affected by faulting, knowing when the fault was last active is important for assessing the safety of the city. The OSL results were compared with radiocarbon dates; the radiocarbon dates were much younger, likely due to contamination from plant materials (Schmidt et al., 2012).

CHAPTER 3. SITES AND SAMPLES

For this study, five alluvial fans were sampled for OSL dating. They are located in Wright Valley, the south side of McKelvey Valley and Bull Pass between Wright and McKelvey Valleys. The five fans are Upper Wright, Jason, Aeolus, Northern Bull and Southern Bull (Figure 3.1).

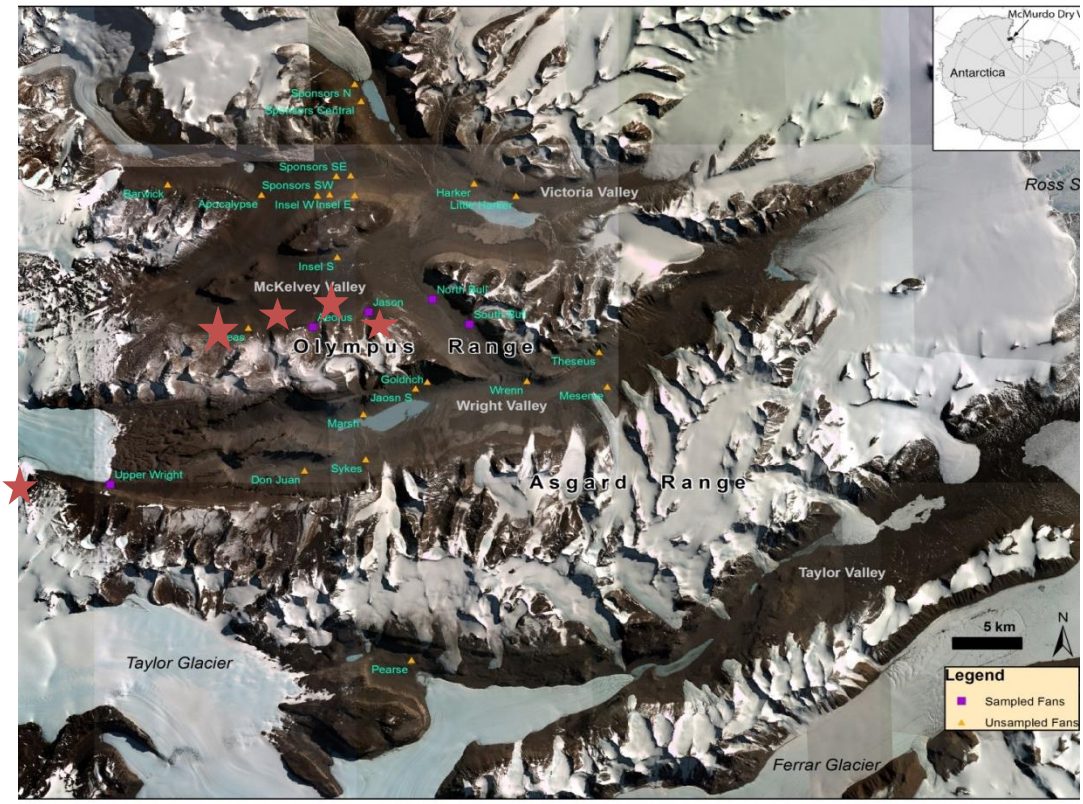

Figure 3.1. Map of the McMurdo Dry Valleys. A number of alluvial fans are labeled; the five fans sampled for this thesis are marked with a red star. The five sampled fans are Aeolus, Jason, Northern Bull Pass, Southern Bull Pass and Upper Wright fan (Zamora, 2013).

Aeolus Fan

Aeolus fan is located to the east of Mt. Aeolus on the western slope of Cartwright Valley (Figure 3.2). The fan is located on a structural bench at an elevation of 1200 m. The central axis is 370 m long. The widest point is 55 m across, and gradually comes to a point at the bottom of

the fan. Meltwater is from a northeast-facing niche glacier at an elevation of 1350 to 1400 m, perched below a structural bench. Meltwater flows through a steep, narrow channel 0.7 km in length with an average gradient of 23% to the fan head.

Three samples from this fan were previously collected and dated by Zamora (2013). Six additional samples were collected and analyzed from three additional pits, FZ1116 (Figure 3.3), FZ1118 (Figure 3.4), and FZ1126 (Figure 3.5).

One sample was analyzed for this thesis from the FZ1116 pit. Two melt packages are present in profile. These rest on till, which is capped by desert pavement. Sample FZ1116bMR was ice-cemented, and obtained at a depth of 20 cm from within the sediments of the lower melt package which consists of planar bedded sands with pebbles.

Four samples were analyzed from pit FZ1118. FZ1118aMR was unconsolidated; the other three samples from this pit were ice-cemented. FZ1118aMR (depth 5 cm) and FZ1118bMR (depth 10 cm) were collected from the upper melt package, consisting of planar bedded sands capped by desert pavement. The middle melt package consisted of massive sands with imbricated cobbles; FZ1118cMR was collected from 25 cm below the surface within this middle package. FZ1118eMR was collected at a depth of 35 cm, just above a buried desert pavement within the lowest melt package in planar bedded sands. Beneath the buried pavement is glacial till.

One sample was analyzed from the FZ1126 pit. The upper melt package is composed of planar bedded sands, adjacent to the modern channel, and capped by the modern desert pavement. There were small sand wedges in this layer. FZ1126b was obtained at a depth of 25 cm from the lower melt package and was ice-cemented. The lower melt package was composed of planar bedded sands overlying the glacial till.

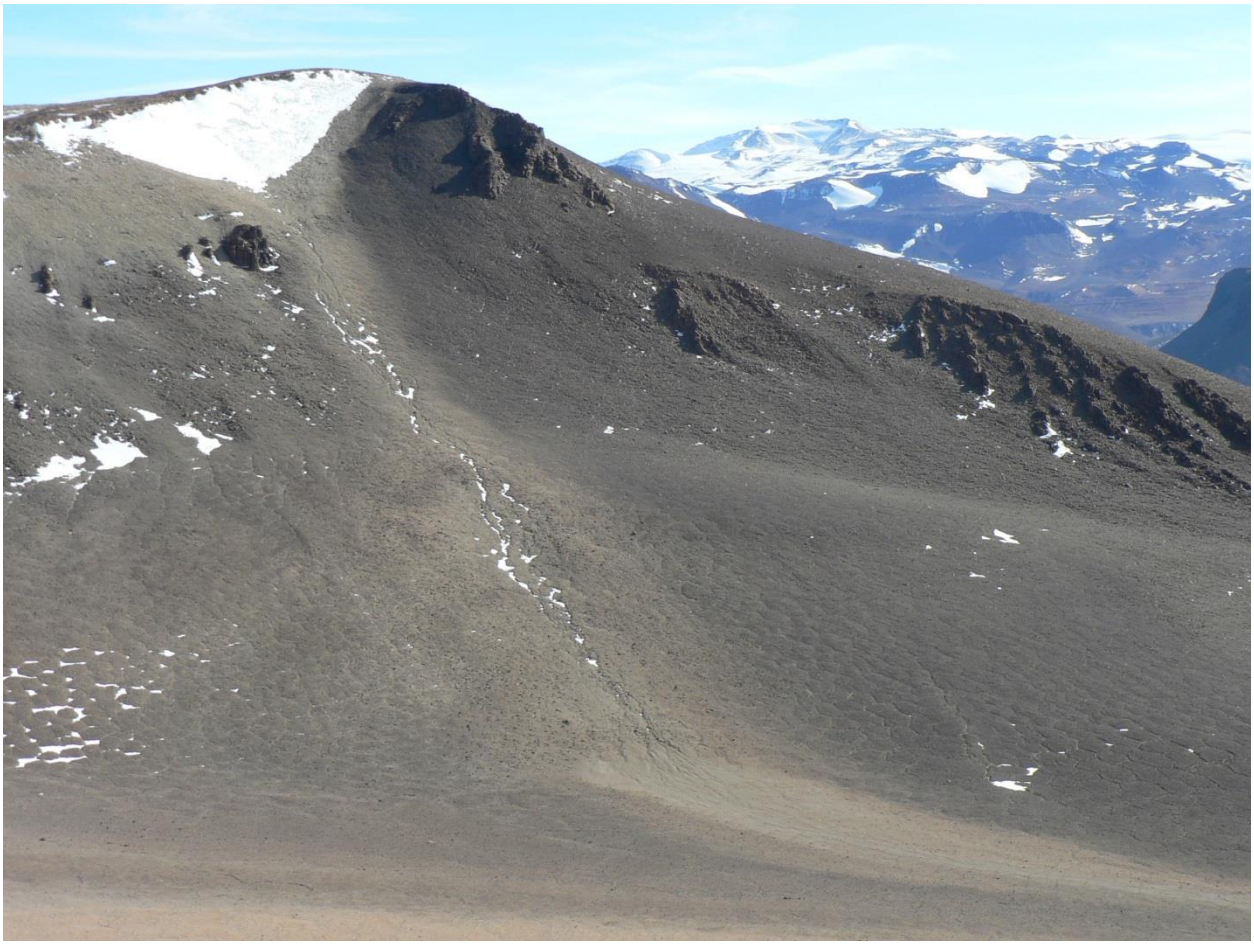

Figure 3.2. Aeolus fan. Aeolus fan is located along the western edge of Cartwright Valley, east of Mt. Aeolus in the Olympus Range. The melt water source is the niche glacier located in an alcove at an elevation of 1400 to 1350 m (photograph curtesy of Felix Zamora).

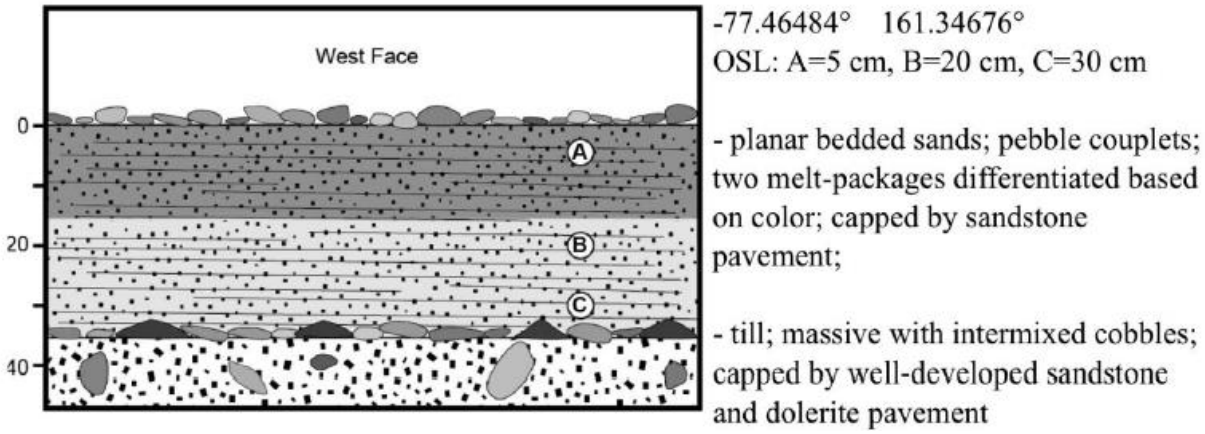

Figure 3.3. Pit sketch Pit FZ1116 on Aeolus fan. The sample FZ1116b was ice-cemented and dated in this project. Pit sketch courtesy of Zamora, 2013.

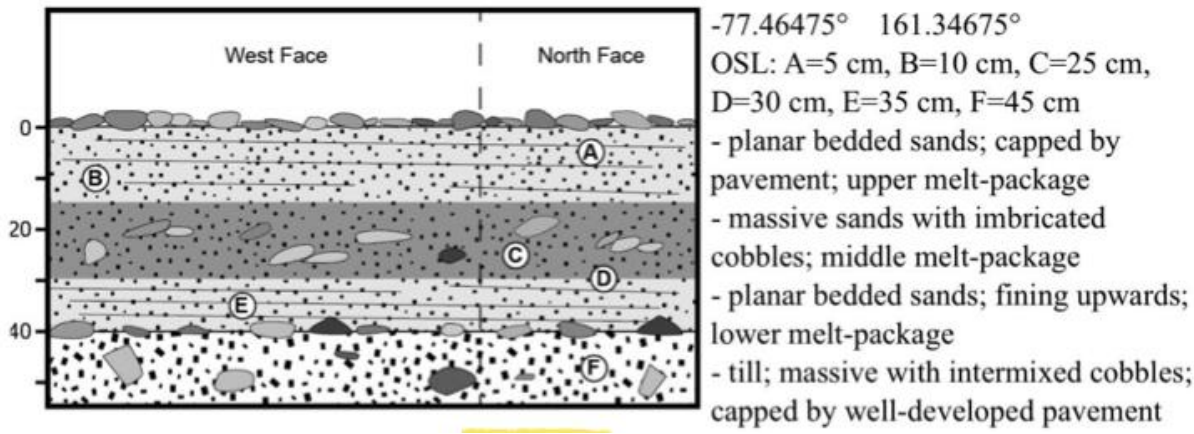

Figure 3.4. Pit sketch for Pit FZ1118MR. FZ1118aMR is the only unconsolidated sample dated from this pit. FZ1118bMR, FZ1118cMR, and FZ1118eMR were ice-cemented. Pit sketch courtesy of Zamora, 2013.

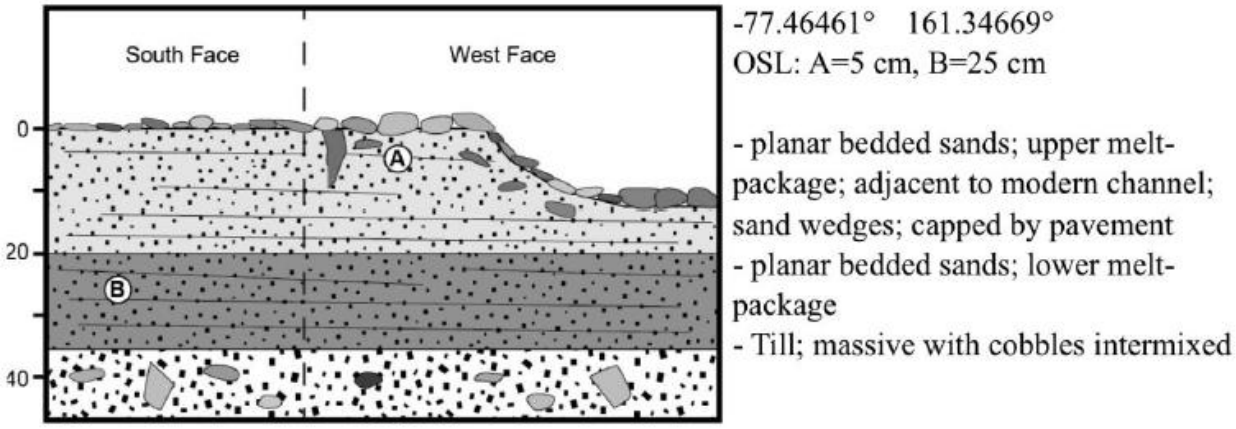

Figure 3.5. Pit sketch for FZ1126. FZ1126bMR was ice-cemented when collected and is the only sample dated from this pit. Pit Sketch courtesy of Zamora, 2013.

Jason Fan

Jason fan is located north of Mt. Jason in the Olympus Range, in the mouth of Bratina Valley (Fig. 3.6). Jason fan is located on a structural bench at an elevation of 1100 m. The fan has a long, narrow profile with a low slope. The fan is 160 m wide and 410 m long along its central axis. Zamora (2013) notes the source of melt water for this fan is a north-facing niche glacier at an elevation of 1350 to 1450 m at the valley head.

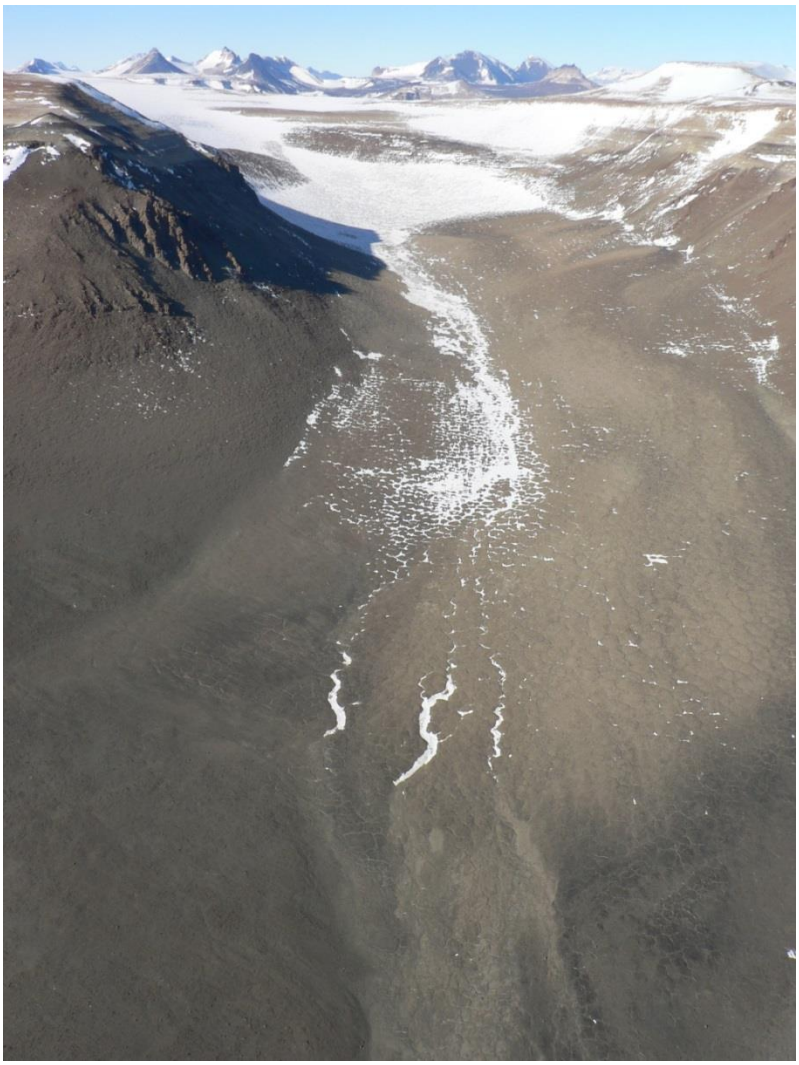

Figure 3.6. Jason fan. Fan is located in the mouth of Bratina Valley, northeast of Mt. Jason in the Olympus range. Image is facing south. Melt water source is the niche glacier at top of the image. Fan is the light colored sediment at the bottom-center of the image (photograph curtesy of Felix Zamora).

Five samples were collected from Jason fan in a pilot study by Lewis and Lepper (unpublished). Three samples from two additional pits were collected during the 2011 field season. FZ1102 was a pit containing weakly-bedded sands with cobbles in the eastern portion, the west face, where the sample was collected consisted of planar bedded sands capped by sandstone and siltstone desert pavement as shown in Figure 3.7 below. The sample from FZ1102 was unconsolidated and collected at a depth of 5 cm. Two samples were collected from pit

FZ1105. FZ1105a was an unconsolidated sample, collected at a depth of 20 cm and included poorly bedded gravelly sands, capped by sandstone and siltstone pavement. FZ1105b was ice-cemented and collected at a depth of 40 cm. The sediment was planar bedded sands. The two samples were possibly separated by a relic desert pavement (see figure 3.8).

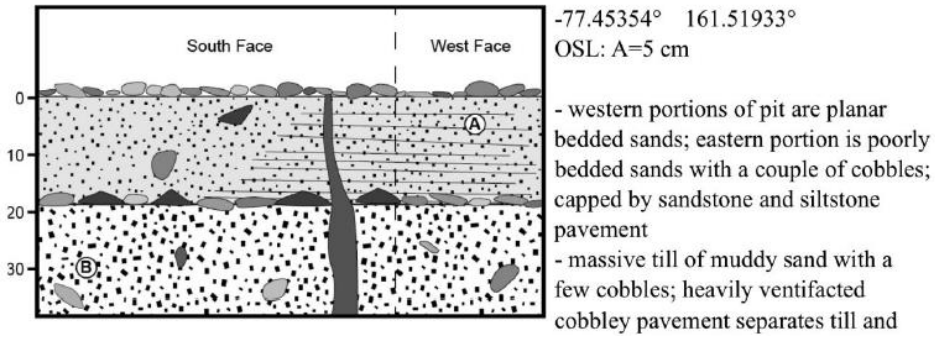

Figure 3.7. Pit sketch from FZ1102 on Jason fan. The sample collected from this pit was unconsolidated. Pit sketch courtesy of Zamora, 2013.

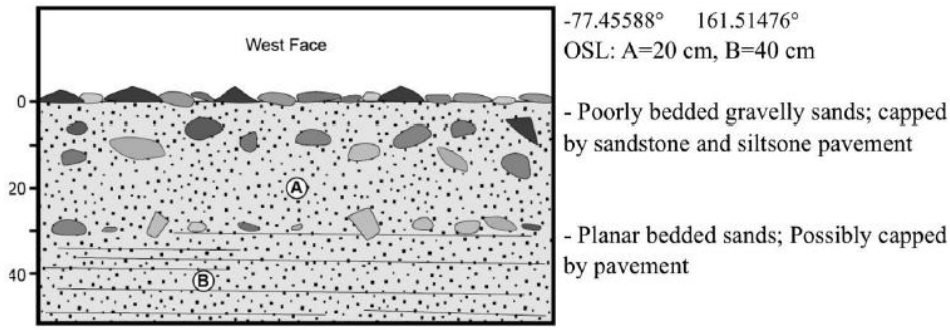

Figure 3.8. Pit sketch for pit FZ1105. FZ1105aMR was unconsolidated, while FZ1105bMR was ice-cemented. Pit sketch is from Zamora, 2013.

Northern Bull Pass Fan

Northern Bull Pass fan is located southwest of Mt. Booth, at the northern end of Bull Pass at an elevation of 700 m (figure 4). The fan extends about 100 m along the central axis, with a width of 85 m along the toe. A southwest facing glacier, with an elevation of 1300 to 1450 m, located to the south of Mt. Booth is the source of melt water for this fan. Water moves from the glacier to the fan through a long (1.8 km), narrow channel with a gradient of 15.7% (Zamora, 2013).

Figure 3.9. Northern Bull Pass fan. Fan is light-colored, fine-grained sediment in center of the image, approximately 85 m wide. Fan is surrounded by glacial till and desert pavements (photograph courtesy of Felix Zamora).

Five samples have been collected and analyzed from Northern Bull Pass fan. FZ1147 had one unconsolidated sample collected at a depth of 5 cm. The pit was in planar bedded sands, which are coarser towards the top of the pit. The surface consists of a granite pavement. The lower portion of the pit contains a granite cobble pavement overlaying massive sands. Pit 1148 had two samples collected. FZ1148a (5 cm below the surface) was dated by Zamora (2013), and FZ1148bMR, collected at 20 cm of depth was dated in this thesis. FZ1148a was unconsolidated, FZ1148b was ice-cemented. The pit is composed of planar bedded gravelly sands with gravel dispersed. The surface is capped by granite pavement.

The pit FZ1150 consisted of planar bedded sands capped by a granite pavement. The alluvial sediments overlay massive sands with intermixed cobbles. Sample FZ1150aMR was collected from the north face of the pit at a depth of 5 cm; the sample was unconsolidated. The

pit FZ1152 contained planar bedded sands topped by a granite pavement. The lower portion of the pit contained massive sands with cobbles and thin sand wedges. An unconsolidated sample, FZ1152aMR was collected at a depth of 5 cm from within this pit.

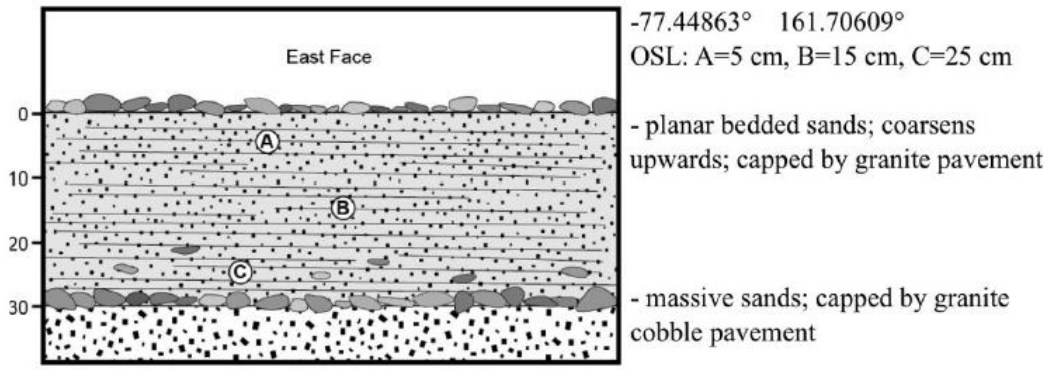

Figure 3.10. The pit sketch for FZ1147 on Northern Bull Pass fan. One unconsolidated sample was collected at a depth of 5 cm. Sketch courtesy of Zamora, 2013.

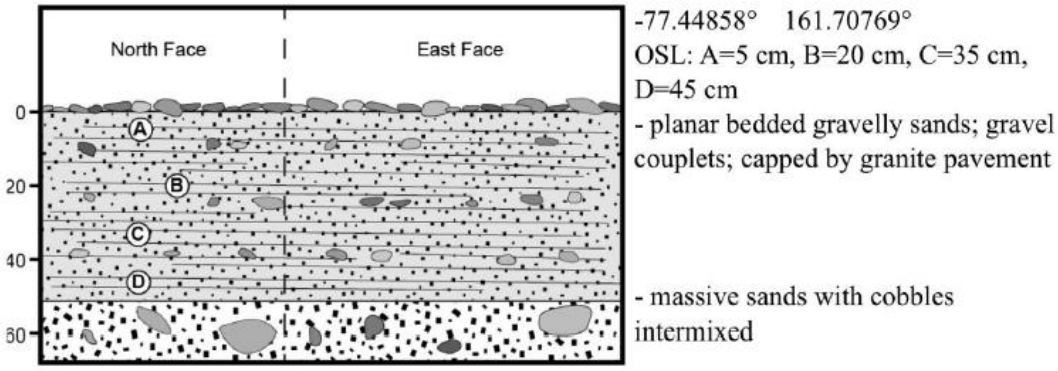

Figure 3.11. Pit sketch for the FZ1148 pit located on Northern Bull Pass fan. One unconsolidated sample (FZ1148a) was collected and dated by Zamora, 2013. A second sample, FZ1148bMR was also collected. Pit sketch is from Zamora, 2013.

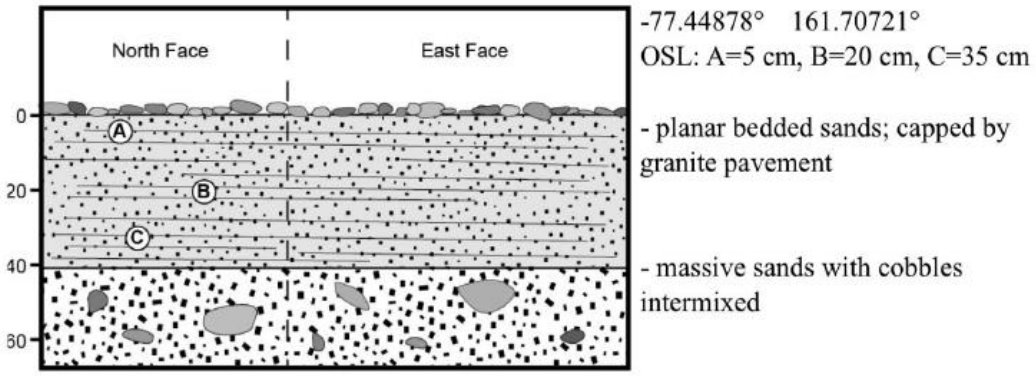

Figure 3.12. The pit sketch for pit FZ1150. FZ1150aMR was an unconsolidated sample collected at a depth of 5 cm. Pit sketch is from Zamora, 2013.

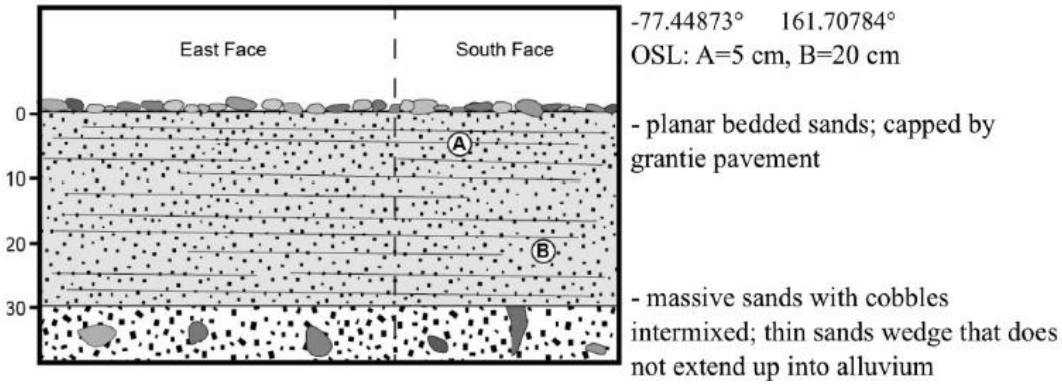

Figure 3.13. Pit sketch for FZ1152 on Northern Bull Pass Fan. One unconsolidated sample was collected from this pit. Pit sketch is courtesy of Zamora, 2013.

Southern Bull Pass Fan

The Southern Bull Pass fan is the largest of the fans in this study (Figure 3.14). The fan is located at the mouth of the Orestes Valley, at an elevation of 650 m. The fan is 1200 m along the central axis and is 1100 m wide at the toe. The fan has a steep upper portion that flattens out halfway down the profile to a broad area with low slope. The melt water source is a south-facing glacier, at an elevation of 1500 m to 1150 m, located in a cirque on the northern slopes of the Orestes Valley. The melt water reaches the fan through a 4.7 km long channel, with an average

gradient of 7.5% (Zamora, 2013). Zamora collected and dated one sample from this fan, from FZ1162.

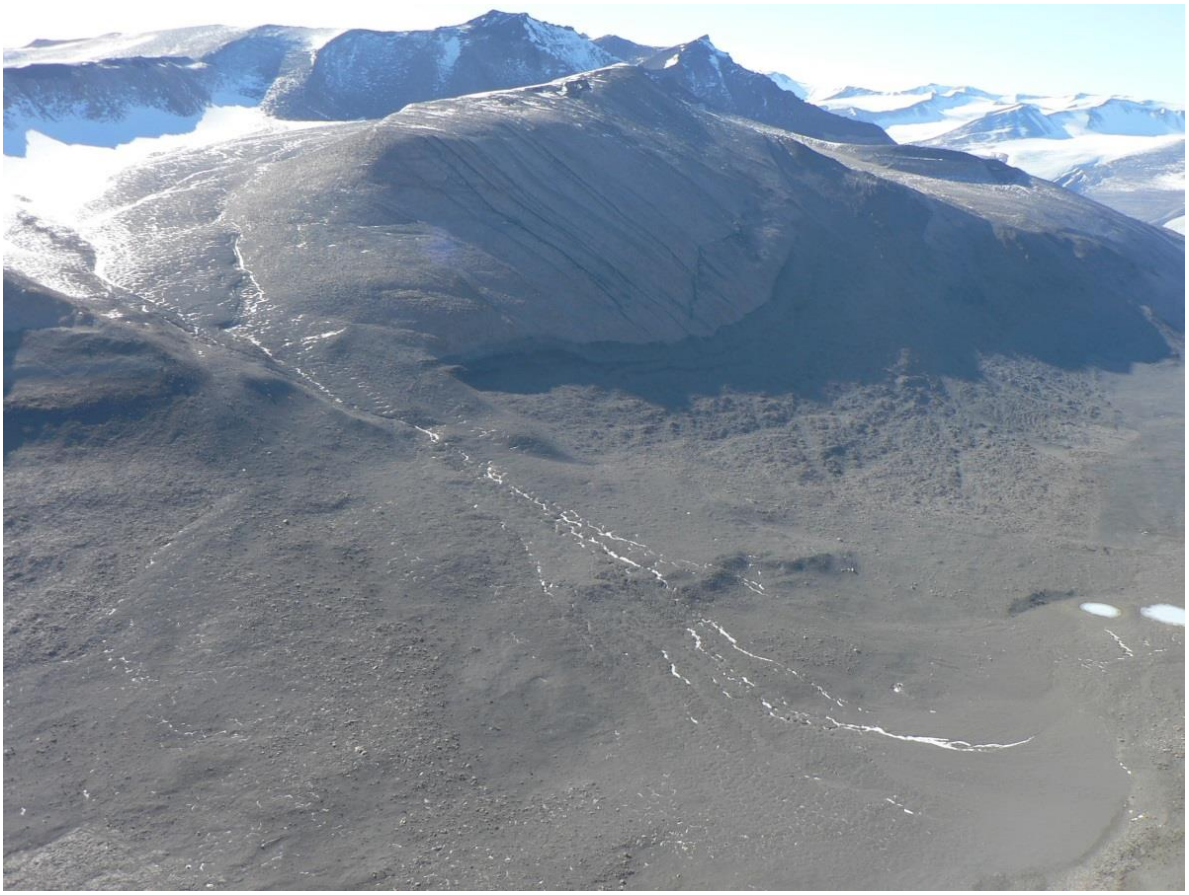

Figure 3.14. Southern Bull Pass fan. The largest of the five studied fans. Melt water source is the south-facing niche glacier in the upper left. Melt water flows through the 4.7 km long channel to the 1100 m wide fan in the lower right corner of the image (photograph curtesy of Felix Zamora).

Upper Wright Fan

Upper Wright fan is located at the head of Wright Valley, northwest of Mt. Thor on the northern slope of the Asgard Range (Figure 3.15). The fan is at an elevation of 900 m. Upper Wright fan is a broad and gently sloped; the central axis is 85 m in length and the toe is 70 m wide (Zamora 2013). At the base of the toe is a small, perennially frozen pond. The melt water source is a north-facing niche glacier, elevation 1125 m to 1000 m, situated below a structural

lip. Melt water arrives at the fan through a 0.6 km channel, with an average gradient of 16.7%.

One sample was collected from Upper Wright fan and dated by Zamora (2013).

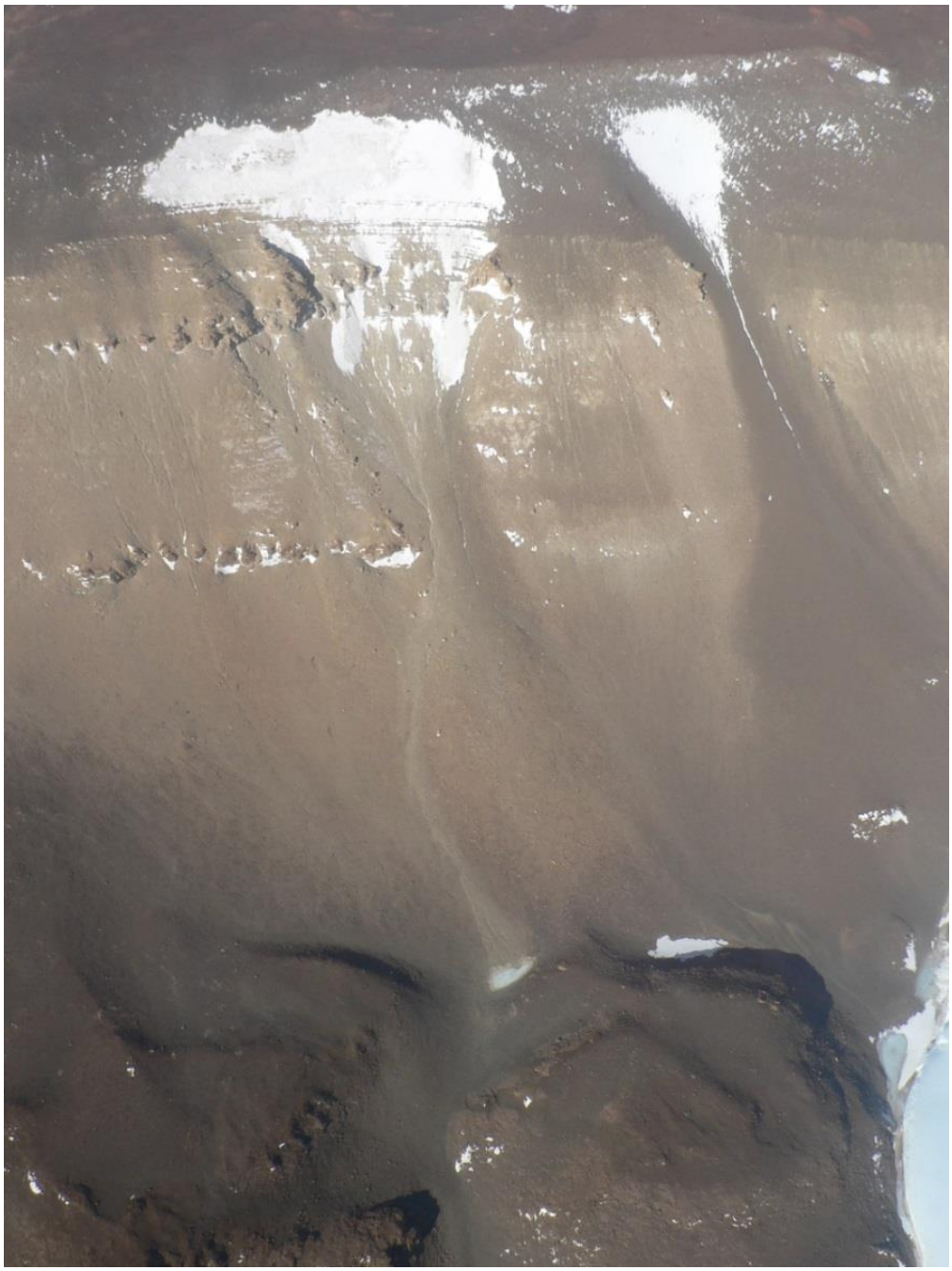

Figure 3.15. Upper Wright fan. The fan is located at the head of Wright Valley, northeast of Mt. Thor in the Asgard range (photograph curtesy of Felix Zamora).

CHAPTER 4. METHODS

Field Sampling and Collection Methods

Sediment samples for OSL dating were collected during the 2011 field season by Zamora, Steffen, and Lewis, using different techniques for ice-cemented and unconsolidated sediments. Fan deposits were ice-cemented at depths below 10 to 40 centimeters beneath the surface. Pit locations were selected to expose thick stratigraphic sequences in the fans, with the expectation of the sequences containing multiple melting events. The pits were excavated to the contact between the alluvial deposits and the Miocene-aged glacial till. The pits were created using hand tools until reaching frozen sediments. Below the frost line, a jackhammer and portable generator were used for further excavation of the pits into the ice-cemented sediment (Figure 4.1). The pits extended as deep as needed to reach the alluvial-till contact, typically 0.5 to 1 m. The pits were designed to disturb as little surface area as possible, typically less than 1 m^2.

For sampling of unconsolidated sediments, a closed-end metal cylinder (7.5 cm diam.) or sealed metal electrical conduit (2.5 cm diam.) was inserted horizontally into the newly exposed pit wall. The pipes and cylinders were then removed and capped in the field, preventing light exposure during transportation.

Ice-cemented sediments were collected using a rotary hammer drill with a concrete coring bit (Figure 4.2). After collection, the entire bit was sealed with duct tape. The cored samples were shipped frozen to the laboratory, where they were stored in a chest freezer until being prepared for OSL dating.

Figure 4.1. Pit Excavation. Pits were excavated using hand tools until reaching ice-cemented (frozen) sediments. Below the frost line, a jackhammer and portable generator were used to excavate the pits to the alluvial-till contact. Photograph courtesy of Adam Lewis.

Figure 4.2. Collection of Ice-cemented sediments. a.)Ice-cemented sediments were collected using a rotary hammer drill with a concrete coring bit. The ice-cemented samples were collected and shipped still frozen to the laboratory. b.) The coring bit in the pit wall. Photographs courtesy of Adam Lewis.

Lab Preparation for OSL Analysis

Unconsolidated samples collected in 7.5 cm diameter cylinders were prepared for grain-size separation and quartz extraction in the light-controlled OSL lab by removing the outermost 2.5 cm of potentially light contaminated sediment. The portion was set aside for elemental analysis. Unconsolidated samples collected in smaller conduit pipe, and the ice-cemented cores were pre-prepared by cutting both ends of the cores off, using a masonry chop-saw with a diamond edged abrasive blade (Figure 4.3). Approximately 2.5 cm was cut off of each end. The sediment in the cut-off ends was set aside for elemental analysis. The ice-cemented core was allowed to thaw before preparation continued. All of the sediment in the small conduit pipes was processed. These samples (collected in conduit pipe) were generally loosely packed, increasing the risk of mixing during handling and transport. Half of the sediment in the ice-cemented cores was processed; the remainder was rewrapped and archived in the same manner as the unconsolidated samples. Thawing adjacent to the cut edges was insignificant, and no heating occurred in the interior of the samples.

Figure 4.3. Preparing ice-cemented samples for processing. The ends of ice-cemented sample drill bits, and the small unconsolidated conduit samples were cut off using a masonry chop saw equipped with a diamond edged abrasive blade.

After removing the sediment from the containers, the next step to preparing samples for OSL analysis is sieving to reach the desired grain size. Sediment larger than 425 μm was discarded. Sediment between 250 to 425 μm was archived in a sealed plastic cylinder. Sediment sized 90-150 μm and 150-250 μm was used for the remaining processing steps. Following sieving, the two smaller grain size fractions were treated with H_2O_2 overnight to remove organic material, and then rinsed (3x) with DI water prior to being treated with HCl overnight to remove carbonates. After being rinsed again (3x) with DI water, the sediment was treated with HF to remove feldspars and etch the surface of the quartz crystals. The sediments were in HF for 45 minutes, alternating between spin mixing and resting every 15 minutes. After another rinse, the 90-150 μm and 150-250 μm sediments were treated with HCl again, to remove fluorides that

could form during HF treatment. Samples were then treated with Na-Pyrophosphate to remove particulates before being rinsed (2x) with methanol and dried. After these chemical treatments, all that should remain is quartz. Before dating measurements, the purity of the processed samples was verified using infrared (IR) prescreening (Spooner and Questiax, 1989).

Data Collection Methods (Extracted with minimal modification from the supplement to Lepper et al., 2007)

All measurements and irradiations were conducted using a Risø DA-15 automated TL/OSL reader system. The system is equipped with a 40 mCi $^{90}Sr/^{90}Y$ ß-source for dose calibrations, which irradiates at a rate 0.1195 Gy/s. Luminescence was stimulated with blue light (470±30 nm) from a diode array and measured with an EMI model 9235QA PMT in the UV emission range (5 mm Hoya U-340). OSL SAR (single aliquot regeneration) data collection procedures (Murray and Wintle, 2000) were used with the minor modification of maintaining a uniform cut-heat and preheat treatments of 160˚C for 10s (Wintle and Murray, 2006; Lepper, 2000; Lepper and McKeever, 2002). Four regeneration doses were used as well as a "check dose" (D_c) to assess the fidelity of dose recovery from each individual aliquot (Lepper and McKeever, 2000). Dose response calibration was conducted for every aliquot and equivalent doses (D_e) were interpolated by linear local slope approximation. Data was collected and analyzed from between 92 and 144 individual sub-samples (aliquots) from each field sample in this investigation.

Dose rates for samples in this investigation were determined from elemental concentrations of K, U, and Th by the method presented by Aitken (1998). Elemental analysis was obtained via instrumental neutron activation (INAA) at the Ohio State University research reactor. Based on collection depth and estimated average water content for each sample the

cosmic ray dose at depth was calculated using the equations of Prescott and Hutton (1988) and Prescott and Hutton (1994).

Paleodose selection

When a distribution of equivalent doses (gD_e) is available from a sample an age representative dose, or Paleodose (D_P) must be selected from the data set. Lepper (2002; Lepper et al., 2002) has shown that the mean and its associated error are not appropriate for data distributions that show strong positive asymmetry resulting from incomplete bleaching or resetting of grains prior to deposition. Most of the D_e data sets in this project were positively asymmetric. This section describes the paleodose selection methods used and the criteria for that selection.

The flow chart shown in Figure 4.4 illustrates the paleodose selection process developed specifically for the Antarctic fans sediments. For symmetric D_e data sets ($M/m < 1.05$), the mean and its associate standard error was used as the paleodose. For the asymmetric D_e data sets ($M/m > 1.05$), the modality of the distribution was used to determine the paleodose selection method. If the D_e distribution was asymmetric and exhibited one mode, the leading edge method was used to determine the paleodose. If the D_e distribution was asymmetric and exhibited two or more distinct modes, the distribution was fitted (or modeled) with the appropriate number of Gaussian equations. The fitted mode and fitted standard error of the lowest dose (most reset) population was then used as the paleodose.

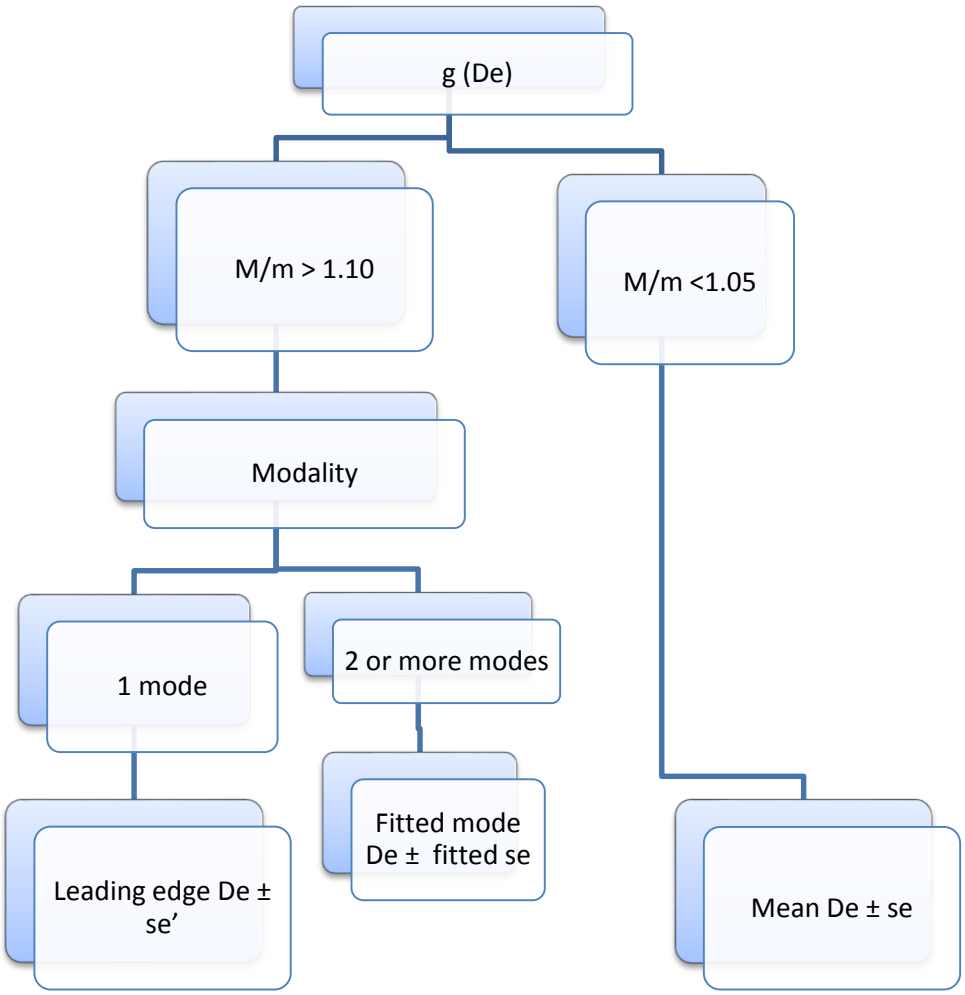

Figure 4.4. Flow chart for paleodose selection.

$$t_{OSL} = \frac{D_p}{D'} \qquad \text{Eqn. 4.1}$$

Ages (t_{OSL}) were then calculated by dividing the paleodose (D_P) by the dose rate (D') for each sample. The ages in this thesis are reported with error and uncertainty, a convention established in Lepper et al., (2011). Age error is the standard error associated with each D_e data set (se, fitted se, or se' as discussed above and depicted in Figure 4.4) divided by the dose rate. Age uncertainty is a fully propagated uncertainty accounting established in Aitken (1985)

CHAPTER 5. RESULTS

Dosimetry

The concentrations of dosimetrically significant elements are shown for each sample in Table 5.1. These data are needed in support of the age calculation as described in the Methods chapter of this thesis. Most of the samples exhibit a very low concentration of K, which suggests a low abundance of K-feldspars in the fan deposits, with the exception of two of the samples from the North Bull Pass fan. Similarly, the concentrations of Th and U are within the typical range observed from quartz-dominated sands.

Table 5.1. OSL Dosimetry Data.

Sample ID	Fan	Depth (cm)	K (ppm)	Rb (ppm)	Th (ppm)	U (ppm)
FZ1102MR	Jason	5	8103 ± 1002	39.88 ± 9.54	3.147 ± 0.296	0.742 ± 0.168
FZ1105aMR	Jason	20	6640 ± 611	45.06 ± 11.57	2.548 ± 0.263	0.711 ± 0.194
FZ1105bMR	Jason	40	8922 ± 627	38.25 ± 5.25	4.754 ± 0.361	0.884 ± 0.071
FZ1116aMR	Aeolus	20	5136 ± 373	25.48 ± 6.13	3.824 ± 0.307	1.219 ± 0.135
FZ1118aMR	Aeolus	5	7792 ± 831	33.79 ± 7.25	3.447 ± 0.294	1.167 ± 0.150
FZ1118bMR	Aeolus	10	5852 ± 513	23.19 ± 7.22	3.321 ± 0.294	1.052 ± 0.182
FZ1118cMR	Aeolus	25	7467 ± 806	40.49 ± 7.62	3.992 ± 0.328	1.025 ± 0.143
FZ1118eMR	Aeolus	35	6322 ± 583	38.07 ± 8.69	3.367 ± 0.294	1.113 ± 0.174
FZ1126bMR	Aeolus	25	8080 ± 981	30.25 ± 10.21	4.561 ± 0.380	1.444 ± 0.212
FZ1147aMR	N. Bull	5	16576 ± 1775	70.51 ± 11.94	7.945 ± 0.627	0.639 ± 0.190
FZ1148bMR	N. Bull	20	8338 ± 739	54.55 ± 13.27	3.967 ± 0.389	1.109 ± 0.366
FZ1150aMR	N. Bull	5	16631 ± 1252	91.20 ± 11.35	5.895 ± 0.472	0.897 ± 0.262
FZ1152aMR	N. Bull	5	8876 ± 822	42.63 ± 11.53	2.810 ± 0.270	0.862 ± 0.303

OSL Ages

The OSL results, including distribution parameters, paleodose and age are summarized in Table 5.2. Thirteen samples were processed for OSL dating, two samples were non-responsive and did not yield dates. One sample was symmetric and was dated using the mean paleodose age. Four samples were dated using the fitted mode paleodose method and the remaining six were dated using the leading edge method.

Jason fan was sampled in two pits. Pit FZ1102 had one unconsolidated sample collected at a depth of 5 cm. The equivalent dose (D_e) distribution for the sample was symmetric (M/m<1.05) and mono-modal (Figure 5.1a). The mean age paleodose selection yielded an age of 8.8 ± 0.4 ka. Pit FZ1105 had two ice-cemented samples collected, FZ1105a at 20 cm, and FZ1105bMR at a depth of 40 cm. FZ1105aMR was dated using the fitted mode paleodose process, and yielded an age of 43.7 ± 3.0 ka. The fitted mode paleodose method was used for FZ1105aMR because the D_e was asymmetric (M/m > 1.10) with two or more modes (Figure 5.1b). FZ1105bMR, was asymmetric (M/m>1.10), mono-modal and yielded a leading edge age of 13.4 ± 1.4 ka (Figure 5.1c).

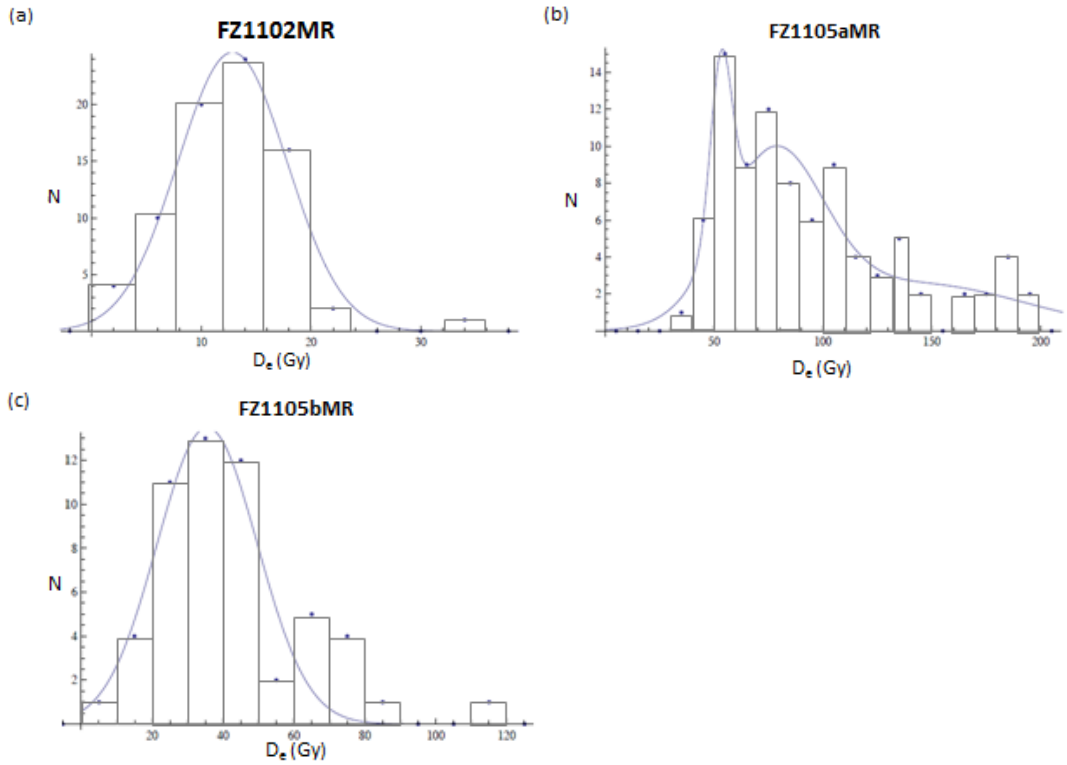

Figure 5.1. The equivalent dose (D_e) distribution for the three samples collected from Jason fan. (a) The D_e distribution for FZ1102MR. (b) The D_e distribution for FZ1105aMR and (c) the D_e distribution for FZ1105bMR.

Six samples were collected from three pits on Aeolus fan. The D_e distributions for all 6 samples from this fan were asymmetric (M/m>1.05) suggesting incomplete solar resetting of the

sediments during transport. Four of the D_e distributions were mono-modal, while two were multimodal. FZ1116bMR was ice-cemented at a depth of 20 cm, and yielded a leading edge age of 4.3 ± 0.3 ka (Figure 5.2a). Four samples were dated from the pit FZ1118. FZ1118aMR was unconsolidated at a depth of 5 cm, and yielded a leading edge age of 2.1 ± 0.2 ka (Figure 5.2b). FZ1118bMR was ice-cemented and collected at a depth of 10 cm. FZ1118bMR was dated using the fitted mode method and yielded an age of 39.9 ± 1.9 ka (Figure 5.2c). FZ1118cMR was ice-cemented at a depth of 25 cm and yielded a leading edge age of 56.7 ± 22.0 ka (Figure 5.2d). The deepest sample dated from pit FZ1118 was FZ1118eMR at a depth of 35 cm. FZ11118eMR had a fitted mode age of 105.9 ± 10.2 ka (Figure 5.2e). The third pit sampled on Aeolus Fan was FZ1126. One sample, FZ1126bMR, was ice-cemented at a depth of 25 cm, and yielded a leading edge age of 4.5 ± 0.7 ka. (Fitted D_e distribution graphic is not available for this sample.)

The third fan, Northern Bull Pass fan, had samples analyzed from four pits. Pit FZ1147 had an unconsolidated sample (FZ1147aMR) collected at a depth of 5 cm that did not yield an age, the sample was non-responsive. Pit FZ1148 had an ice-cemented sample (FZ1148bMR) collected at a depth of 20 cm that was also non-responsive and did not yield an age. Pit FZ1150 had an unconsolidated sample, FZ1150aMR, collected at a depth of 5 cm that yielded a fitted mode age of 11.1 ± 0.4 ka. FZ1150aMR had a D_e that was asymmetric (M/m>1.10) and multimodal (Figure 5.3a). Pit FZ1152 had one sample dated from it. FZ1152aMR was an unconsolidated sample collected 5 cm below the surface, using the fitted mode method, an age of 9.0 ± 0.1 ka (Figure 5.3b). Both samples had D_e distributions that were asymmetric and multimodal.

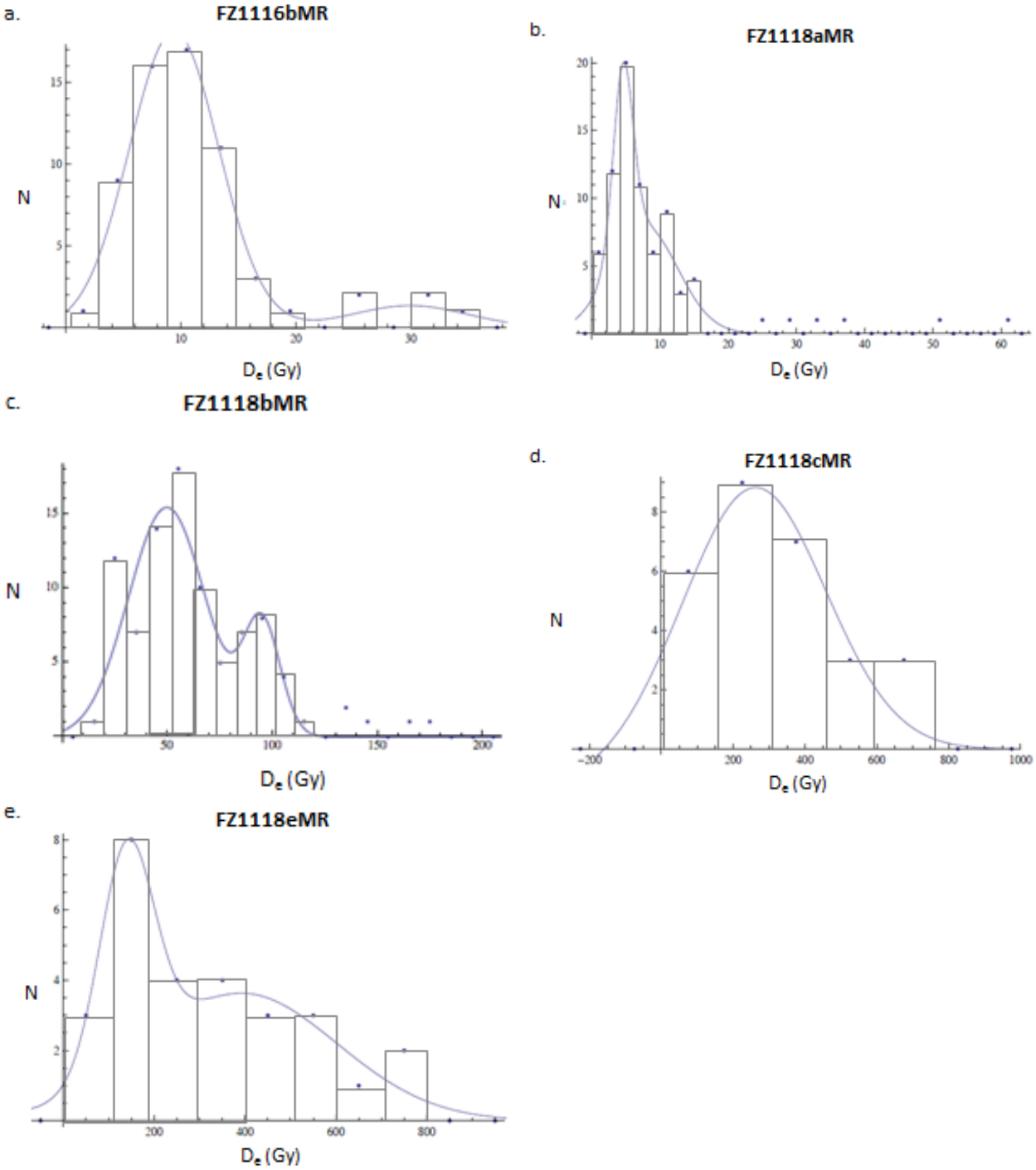

Figure 5.2. The equivalent dose (D_e) distributions for the samples collected on Aeolus fan. a.) The single mode distribution for FZ1116bMR. b.) The D_e distribution for FZ1118aMR. C.) The single-mode D_e distribution for FZ1118bMR. d.) The D_e distribution for FZ1118cMR was also single-mode. e.) FZ1118eMR has an equivalent dose distribution that is multi-modal, leading to it being dated using the fitted mode method.

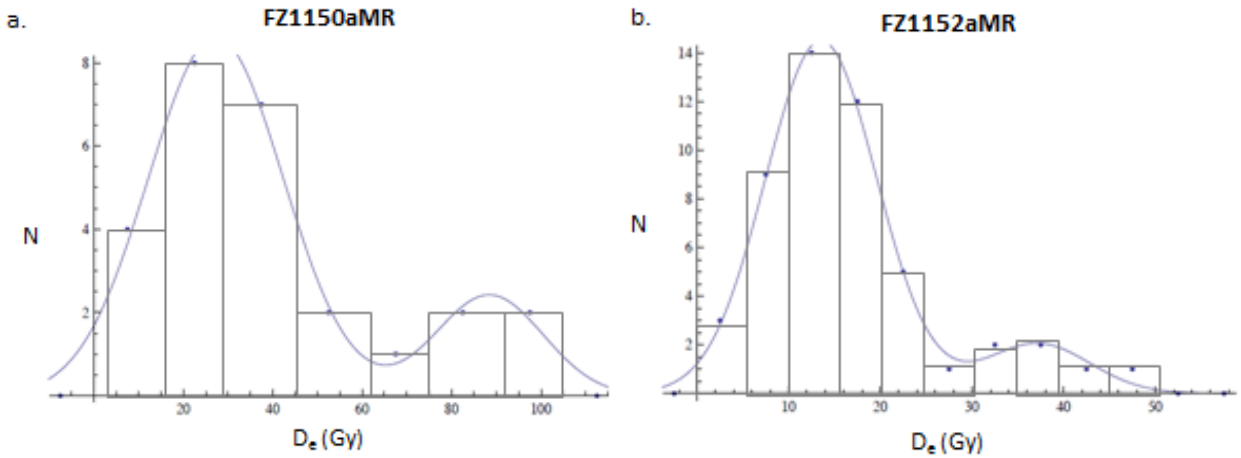

Figure 5.3. The equivalent dose (D_e) distributions for samples dated from Northern Bull Pass fan. a.) The multi-modal distribution for FZ1150aMR. b.) The multi-modal distribution for FZ1152aMR, dated using the fitted mode method.

Table 5.2. OSL Dating Results.

Sample ID	Fan	H_2O state*	Depth (cm)	N	□Dc (%)	M/m	modality	Paleo-dose basis**	Paleodose (J/kg)	Dose Rate (J/kg/ka)	OSL Age (ka)	Age Uncert (ka)
FZ1102MR	Jason	uncon.	5	77/95	1.0	0.94	single	mean	12.007 ± 0.587	1.372 ± 0.141	8.8 ± 0.4	1.0
FZ1105aMR	Jason	ice-cem.	20	91/95	3.2	1.15	multiple	fitted	51.163 ± 3.486	1.170 ± 0.110	43.7 ± 3.0	5.3
FZ1105bMR	Jason	ice-cem.	40	54/119	2.2	1.12	single	D_{LE}	21.345 ± 1.725	1.534 ± 0.101	13.4 ± 1.1	1.4
FZ1116bMR	Aeolus	ice-cem.	20	64/96	10.0	1.09	single	D_{LE}	5.320 ± 0.380	1.231 ± 0.118	4.5 ± 0.3	0.5
FZ1118aMR	Aeolus	uncon.	5	77/143	12.6	1.52	single	D_{LE}	3.025 ± 0.219	1.460 ± 0.125	2.1 ± 0.2	0.2
FZ1118bMR	Aeolus	ice-cem.	10	93/96	4.4	1.11	multiple	D_{LE}	49.552 ± 2.396	1.241 ± 0.105	39.9 ± 1.9	3.9
FZ1118cMR	Aeolus	ice-cem.	25	24/142	0.6	1.17	single	D_{LE}	79.624 ± 30.946	1.404 ± 0.119	56.7 ± 22.0	22.5
FZ1118eMR	Aeolus	Ice-cem.	35	29/118	14.0	1.15	multiple	fitted	134.15 ± 12.91	1.267 ± 0.103	105.9 ± 10.2	13.3
FZ1126bMR	Aeolus	ice-cem.	25	86/96	1.1	1.63	single	D_{LE}	7.191 ± 1.141	1.590 ± 0.141	4.5 ± 0.7	0.8
FZ1147aMR	N. Bull	uncon.	5	- - -	- - -	- - -	- - -	n/a	Non-responsive	- - -	- - -	- - -
FZ1148bMR	N. Bull	ice-cem.	20	- - -	- - -	- - -	- - -	n/a	Non-responsive	- - -	- - -	- - -
FZ1150aMR	N. Bull	uncon.	5	27/119	12.0	1.23	multiple	fitted	26.229 ± 0.921	2.365 ± 0.180	11.1 ± 0.4	0.9
FZ1152aMR	N. Bull	uncon.	5	57/118	7.7	1.53	multiple	fitted	13.023 ± 0.178	1.446 ± 0.145	9.0 ± 0.1	0.9

*uncon., unconsolidated; ice-cem., ice-cemented

**mean, mean ± se; fitted, fitted mode ± fitted se; D_{LE}, leading edge dose ± se' (Supplement to Lepper et al., 2007).

CHAPTER 6. DISCUSSION

This chapter explores the correlation among fan deposits and to climate drivers as interpreted by the available OSL ages. The ages of each sample dated in this thesis are shown in the simplified stratigraphic columns below. Jason fan had three samples dated from two pits (Figure 6.1). The pit FZ1105 shows an age inversion, with the FZ1105a sample having an age of 43.7 ± 3.0 ka and the FZ1105b sample is 13.4 ± 1.4 ka. A possible explanation for the age inversion can be found in the sedimentology of the pit. The lower sample (FZ1105b) was composed of the planar bedded sands typical of an alluvial fan. The upper sample (FZ1105a) was composed of poorly bedded gravelly sands, likely deposited in a debris flow. Because sediments in a debris flow are often not exposed to sufficient sunlight before deposition, the sediments are not fully zeroed, so the age represents inheritance from a prior deposition period.

The Aeolus fan had six samples dated from three pits (Figure 6.2). The FZ1118 pit had four samples collected, showing a strong chronostratigraphic sequence. The youngest sample in this pit was 2.1 ka, while the oldest was 105.9 ka. The Northern Bull Pass fan had four pits, two samples were non-responsive (Figure 6.3). The non-responsive results were due to the samples having extremely low signals, which is a common problem in Antarctic samples (discussed in literature review as well as Lepper, 2011, *pers. comm*.).

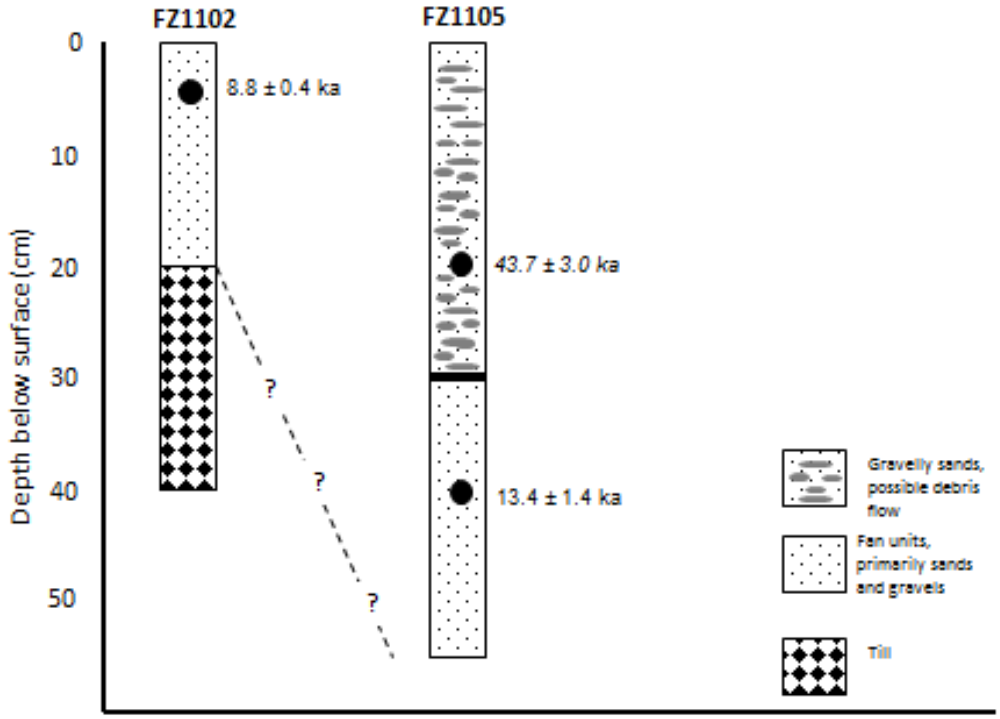

Figure 6.1. Jason fan age results. Units/sediments are described in chapter 2 of this thesis and in greater details in Zamora (2013).

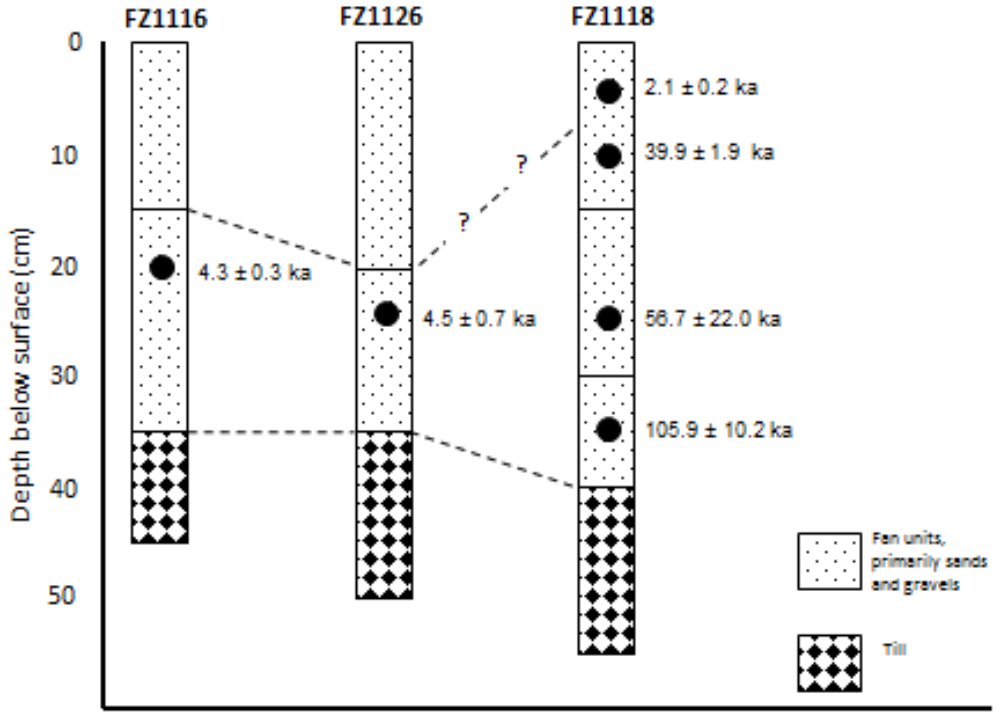

Figure 6.2. Aeolus fan age results. Units/sediments are described in chapter 2 of this thesis and in greater details in Zamora (2013).

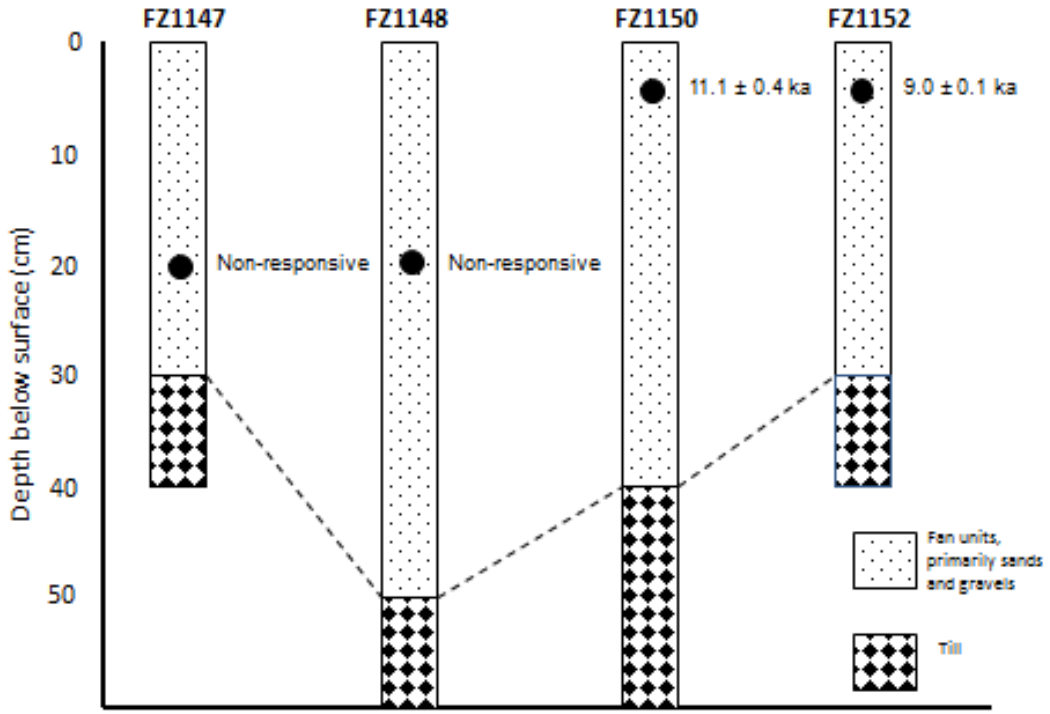

Figure 6.3. Northern Bull Pass fan age results. Units/sediments are described in chapter 2 of this thesis and in greater details in Zamora (2013).

Integrated Results

Twenty four samples have been dated from five alluvial fans in the McMurdo Dry Valleys. The ages for all the available samples are listed below in Table 6.1. Thirteen of the samples are from this thesis, five are from Lewis and Lepper (unpublished) and the remainder comes from Zamora (2013). The samples range in age from 1.1 ka to 105.9 ka.

Table 6.1. The ages of all alluvial sediments dated in this study. The samples are ordered chronologically from youngest to oldest.

Sample ID	Fan	Depth (cm)	OSL Age (ka)	Age Error (ka)	Source
FZ1142	Aeolus	5	**1.1**	0.1	Zamora, 2013
FZ1148a	N. Bull	5	**1.3**	0.3	Zamora, 2013
FZ1118aMR	Aeolus	5	**2.1**	0.2	This thesis
FZ1134a	Aeolus	5	**2.3**	0.3	Zamora, 2013
FZ1158a	S. Bull	10	**2.3**	0.3	Zamora, 2013
FZ1162	Up. Wright	4	**2.5**	0.1	Zamora, 2013
FZ1134b	Aeolus	10	**3.1**	0.3	Zamora, 2013
FZ1116bMR	Aeolus	20	**4.3**	0.3	This thesis
FZ1126bMR	Aeolus	25	**4.5**	0.3	This thesis
ALE0860cKL	Jason	19	**6.1**	1.6	Lewis, Lepper; pilot study
ALE0860dKL	Jason	10	**8.1**	1	Lewis, Lepper; pilot study
FZ1102MR	Jason	5	**8.8**	0.4	This thesis
FZ1152aMR	N. Bull	5	**9.0**	0.1	This thesis
ALE0861KL	Jason	12	**9.7**	0.8	Lewis, Lepper; pilot study
FZ1150aMR	N. Bull	5	**11.1**	0.4	This thesis
FZ1105bMR	Jason	40	**13.4**	1.1	This thesis
ALE0860bKL	Jason	31	**14.1**	1.7	Lewis, Lepper; pilot study
FZ1118bMR	Aeolus	10	**24.4**	1.6	This thesis
FZ1105aMR	Jason	20	**43.7**	3	This thesis
FZ1118cMR	Aeolus	25	**56.7**	22	This thesis
ALE0860aKL	Jason	31	**63.8**	5	Lewis, Lepper; pilot study
FZ1118eMR	Aeolus	35	**105.9**	10.2	This thesis
FZ1147aMR	N. Bull	5	**- - -**	**- - -**	This thesis
FZ1148bMR	N. Bull	20	**- - -**	**- - -**	This thesis

Periods of increased alluvial fan activity in the Dry Valleys are clustered around 1-3 ka, and 8 to 11 ka (Figure 6.4). There are not enough samples older than 11 ka to determine if additional periods of clustering occur. For the most recent period of fan activity, occurring in the late Holocene, nine of the 24 samples are dated as younger than 4.5 ka. All fans except Jason show deposition during this period. For the cluster occurring in the Pliestocene/Holocene transition, five samples were dated with ages between 8.1 and 11.1 ka.

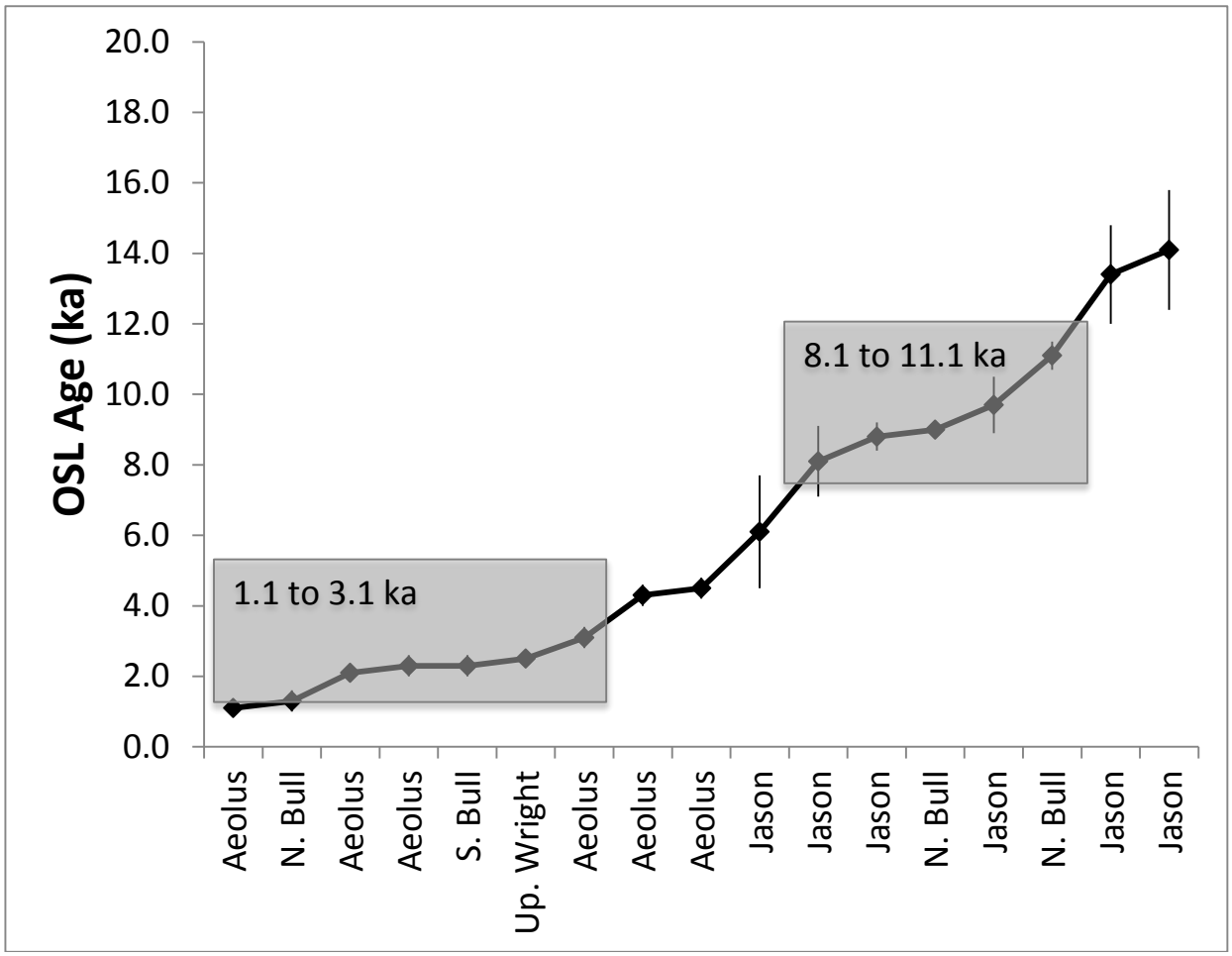

Figure 6.4. Clustering of fan activity. Clusters of increased fan activity occur from 1.1 to 3.1 ka and 8.1 to 11.1 ka.

Interpretations

Peter Huybers has proposed that the length of summer is more important for increased melting than the intensity of the summer in Antarctica (Huybers and Denton, 2008). Insolation is the amount of sunlight an area receives over a length of time. Insolation is more intense during the summer. In Antarctica, sunlight is only received during the spring, summer and fall. To evaluate the potential relationship between fan activity and insolation, three insolation curves were created using a program called AnalySeries, available from the University of Versailles. The curves show the amount of insolation occurring at 78°S (the latitude of the Dry Valleys)

over various periods of time. One curve shows the mean insolation over the last 40,000 years, the next curve shows the mean annual insolation over the last 100,000 years. The third curve shows the insolation received on a specific day each year for the last 40,000 years.

The 40,000 year mean annual insolation curve is shown in Figure 6.5 below. The peak mean insolation occurred 10,000 years ago. This matches well with the cluster of fan activity that occurred between 8,000 and 11,000 years ago. The melting events recorded during that period are likely related to the longer period of sunlight exposure. The summers at that time may not have been as intense but there were more days of solar irradiation. The length of summer is related to precession, the 21,000 year cycle that changes the orientation of Earth's rotational axis relative to the sun. The precessional cycle affects the tilt of the earth. When the tilt places the Northern hemisphere closest to the sun, during the time when the Earth is passing closest to the sun (perihelion), then the Earth is at its furthest location in the orbit around the sun (aphelion) during the Southern hemisphere summer. The Earth does not orbit the sun in a perfect circle, its orbit is more elliptical shaped, so the Earth can be different distances from the sun at different points in the year. The distance from the sun, and the tilt of the Earth combined affect the amount of solar radiation during the summer. Aphelion leads to a less intense solar radiation during the longer summer and shorter winter (Huybers, 2009). During the period of peak mean annual insolation 10,000 years ago, aphelion was occurring during the Antarctic summer, leading to the melting events recorded in the alluvial fans in this study.

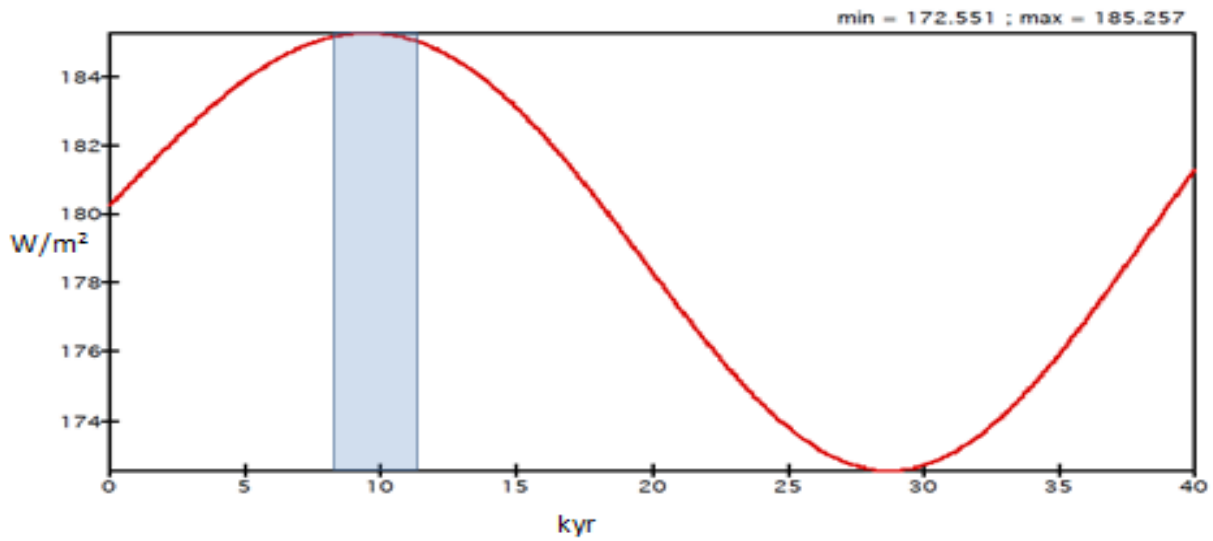

Figure 6.5. The 40 kyr mean annual insolation curve. The mean annual insolation curve for 78 ° S, showing the average insolation received in the McMurdo Dry Valleys over the last 40 kyr. The peak insolation occurred around 10,000 years ago. The boxes indicate clusters of fan activity occurring between 8.1-11.1 kyr and 1.1 to 3.1 kyr.

A second mean annual insolation curve was plotted to show the average insolation over the last 100,000 years to see how well the earlier melting events correlate with periods of longer, less intense summers (Figure 6.6). The earliest melting event recorded in this data set occurred 105.9 ka and is not shown on the insolation curve. Individual events occurring between 13.1 ka and 63.8 ka are marked on the curve with individual vertical lines. Melting events occurred 64,000 and 57,000 years ago, at those times, insolation was increasing from the minimum mean insolation period that occurred 70,000 years ago. Melting events occurred both before and after the period of peak insolation (48,000-50,000 years ago), but no events were recorded at the time of peak insolation. Melting events may still have occurred at peak insolation, but due to how sediment is deposited on the fans and how sampling occurred, those events are not represented in this data set.

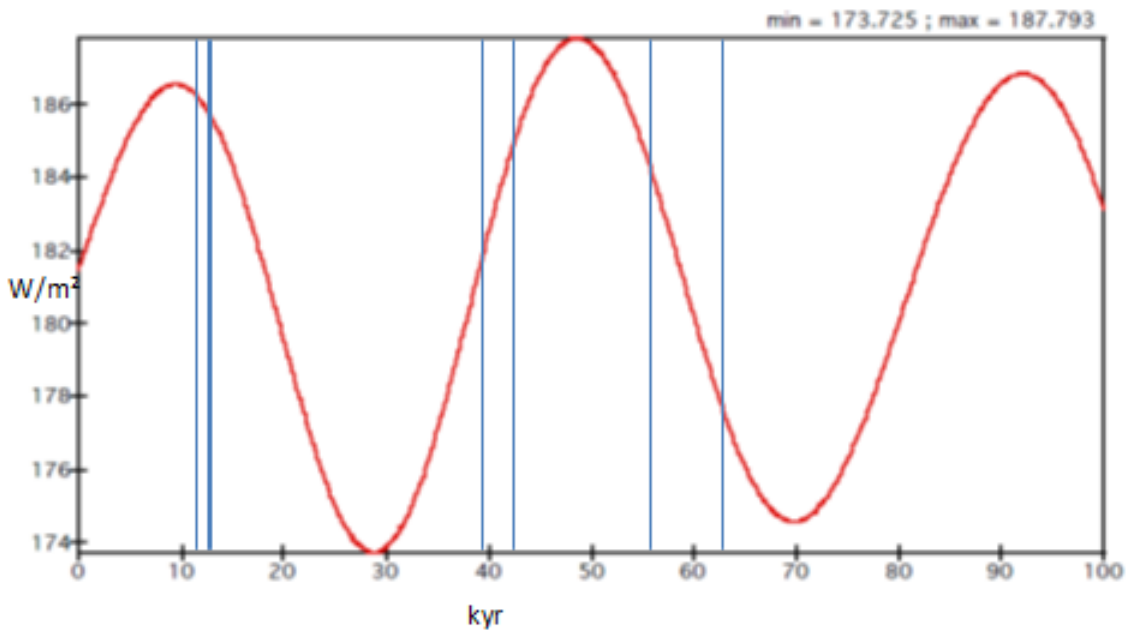

Figure 6.6. The 100 kyr mean annual insolation curve. The insolation curve for the McMurdo Dry Valleys (78° S) showing mean annual insolation over the last 100,000 years. The lines indicate individual melting events occurring between 13,100 and 63,800 years ago, the individual melting events all occur at times of near peak insolation.

The two mean insolation curves can be compared to a daily insolation curve, which plots the amount of insolation received at 78° South on a given day (day 300/January 21) over the past 40,000 years. Daily insolation shows the intensity of insolation, which reflects periods of increased solar radiation, due to greater tilt of the Earth's axis (Obliquity). Obliquity varies on a 41,000 year cycle. When the axis is tilted at a greater angle, more radiation is received during the Southern hemisphere summer, leading to a summer with increased daily insolation. The daily insolation curve below shows the insolation occurring in mid-January (Figure 6.7). Peak daily insolation occurred in the Dry Valleys about 18,000 years ago, and melting events are not recorded at that time. At 10,000 years ago, there was a period of relatively low daily insolation, showing that the melting events recorded in the alluvial fans are likely more related to mean annual insolation (and precession) than to daily insolation (and obliquity). Daily insolation began

increasing about 5000 years ago through the present time. A cluster of fan activity occurs from 1 to 3 ka with additional melting events from 4.3 to 6.1 ka. During the most recent periods of fan activity, daily insolation in January was at its most intense, leading to warmer temperatures and melting.

Based on these preliminary modeling efforts, we interpret that insolation is well correlated to depositional events on high elevation fans in the Antarctic Dry Valleys. However, insolation is a more complex driver than simply mean annual insulation. Intensity during a given summer and length of given summer may also be able to drive small scale melting events in this region.

OSL ages for the alluvial deposits in the McMurdo Dry Valleys were internally coherent and showed stratigraphic consistency within the pits. Depositional units were able to be correlated between pits on the individual fans. Depositional activity on the fans can be linked to insolation, with fan activity occurring during periods of high mean annual insolation.

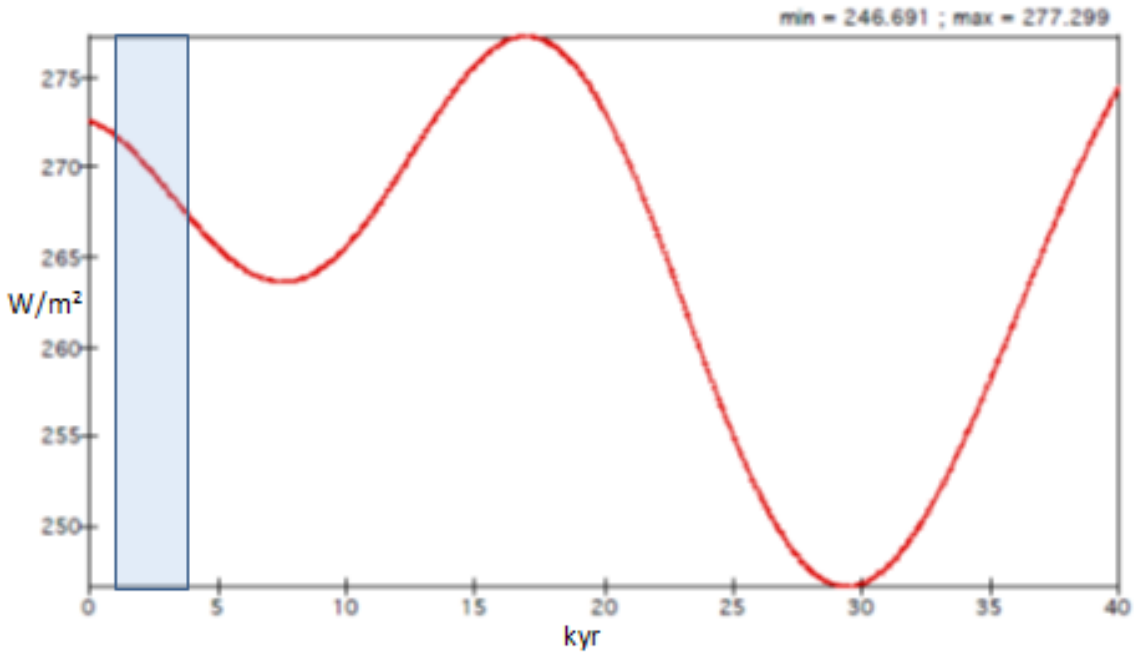

Figure 6.7. The daily insolation curve for the McMurdo Dry Valleys (78° S) over the last 40,000 years. The curve was calculated using AnalySeries to determine the daily insolation occurring on day 300 (January 21) every year.

CHAPTER 7. CONCLUSIONS

High-elevation alluvial fans in the McMurdo Dry Valleys of Antarctica were evaluated as archives of occasional melting events along glacial margins. The overall goal of the project was to determine if these small fans could be used as an archive for climate proxy data in this region of Antarctica. In order to accomplish that goal, sediment samples from the fans were dated using Optically Stimulated Luminescence (OSL) and the results were correlated with insolation curves.

The fans are composed primarily of planar bedded sands and were ice-cemented below 10 to 40 cm. Sediment samples were collected by Zamora, Steffen and Lewis from five alluvial fans during the 2011-2012 field season. Unconsolidated samples were collected using metal cylinders or conduit pipe. Ice-cemented samples were collected using a portable jack hammer and rotary hammer drill equipped with a concrete coring bit. Ice-cemented samples were transported frozen to the lab where the light-exposed ends were cut off core was minimal, with no appreciable internal heating.

A total of thirteen samples from three fans were dated for this thesis using OSL dating. Ages were determined using either the mean, fitted mode, or leading edge methods; depending on whether the dose distribution was symmetrical or asymmetrical and the number of modes in the distribution. Ages ranged from ~2.1 to ~110 ka. Two samples were non-responsive due to extremely low signals. There was an age inversion in one pit, due to debris flow deposits in a higher stratigraphic position not being completely reset.

When the OSL results from this thesis were combined with the results from Zamora (2013) and Lewis & Lepper (unpublished), a total of twenty-four samples were dated. Ages ranged from 1.1 to 110 ka. Clusters of fan activity occurred between 1.1 and 3.1 ka and 8.1 to

11.1 ka. No clustering could be identified further back in time due to the small number of older samples collected and dated.

Melting events on the glacial margins above these fans seem to correlate to mean annual insolation. Fan activity is related to periods of longer summers with less intense sunlight. Peak mean annual insolation occurred 10,000 years ago, which aligns well with the cluster of activity between 8.1 and 11.1 ka.

High-elevation alluvial fans in the McMurdo Dry Valleys show promise as an archive of climate proxy data in Antarctica. The alluvial sediment is deposited in discrete melting events on nearby glaciers. Future work in this area could involve looking at how the periods of fan activity correlate with other factors influencing climate in the Dry Valleys, such as the amount of sea ice covering the nearby Ross Sea. More samples need to be dated from deep pits to see how well older melting events correlate with mean annual insolation.

REFERENCES

Aitken, M. J., 1985, Thermoluminescence Dating: London, Academic Press.

Aitken, M. J., 1998, An Introduction to Optical Dating: New York, Oxford University Press.

Arnold, L. J., and R. G. Roberts, 2011, Paper I - Optically stimulated luminescence (OSL) dating of perennially frozen deposits in north-central Siberia: OSL characteristics of quartz grains and methodological considerations regarding their suitability for dating: Boreas, v. 40, p. 389-416.

Arnold, L. J., R. G. Roberts, R. D. E. Macphee, J. S. Haile, F. Brock, P. Moller, D. G. Froese, A. N. Tikhonov, A. R. Chivas, M. T. P. Gilbert, and E. Willerslev, 2011, Paper II - Dirt, dates and DNA: OSL and radiocarbon chronologies of perennially frozen sediments in Siberia, and their implications for sedimentary ancient DNA studies: Boreas, v. 40, p. 417-445.

Arnold, L. J., R. G. Roberts, R. D. E. MacPhee, E. Willerslev, A. N. Tikhonov, and F. Brock, 2008, Optical dating of perennially frozen deposits associated with preserved ancient plant and animal DNA in north-central Siberia: Quaternary Geochronology, v. 3, p. 114-136.

Bacon, S. N., E. V. McDonald, T. G. Caldwell, and G. K. Dalldorf, 2010, Timing and distribution of alluvial fan sedimentation in response to strengthening of late Holocene ENSO variability in the Sonoran Desert, southwestern Arizona, USA: Quaternary Research, v. 73, p. 425-438.

Ballantyne, C. K., 2002, Paraglacial Geomorphology: Quaternary Science Reviews, v. 21, p. 1935-2017.

Berger, G. W., P. T. Doran, and K. J. Thomsen, 2010a, Single-grain and multigrain luminescence dating of on-ice and lake-bottom deposits at Lake Hoare, Taylor Valley, Antarctica: Quaternary Geochronology, v. 5, p. 679-690.

Berger, G. W., S. Ante, and E. Domack, 2010b, Luminescence from glacimarine sediment-trap samples at the Antarctic Peninsula: Quaternary Geochronology, v. 5, p. 244-249.

Berger, G. W., S. Ante, and E. W. Domack, 2009, Seasonal and water-depth variations in sediment luminescence and in sedimentation from sediment trap samples at Gerlache Strait, Antarctic Peninsula: Antarctic Science, v. 21, p. 483-499.

Berger, G. W., and P. T. Doran, 2001, Luminesence-dating zeroing tests in Lake Hoare, Taylor Valley, Antarctica: Journal of Paleolimnology, v. 25, p. 519-529.

Berger, G. W., P. T. Doran, and K. J. Thomsen, 2013, Micro-hole and multigrain quartz luminescence dating of Paleodeltas at Lake Fryxell, McMurdo Dry Valleys (antarctica), and relevance for lake history: Quaternary Geochronology, v. 18, p. 119-134.

Blair, T. C., and J. G. McPherson, 1994, Alluvial fans and their natural distinction from rivers based on morphology, hydraulic processes, sedimentary processes, and facies assemblages: Journal of Sedimentary Research, p. 450-489.

Bøtter-Jensen, L., 1997, Luminescence techniques: Instrumentation and methods: Radiation Measurements, v. 27, p. 749-768.

Bristow, C. S., P. C. Augustinus, I. C. Wallis, H. M. Jol, and E. J. Rhodes, 2010, Investigation of the age and migration of reverseing dunes in Antarctica using GPR and OSL, with implications for GPR on Mars: Earth and Planetary Science Letters, v. 289, p. 30-42.

Bull, W. B., 1977, The alluvial-fan environment: Progress in Physical Geography, p. 222-270.

Catto, N. R., 1993, Morphology and Development of an alluvial fan in a permafrost region, Aklavik range, Canada: Geografiska Annular, v. 75, p. 83-93.

Crosta, G. B., and P. Frattini, 2004, Controls on modern alluvial fan processes in the central Alps, northern Italy: Earth Surface Processes and Landforms, v. 29, p. 267-293.

De Chant, L. J., P. P. Pease, and V. P. Tchakerian, 1999, Modelling alluvial fan morphology: Earth System Processes and Landforms, v. 24, p. 641-652.

DeLong, S. B., and L. J. Arnold, 2007, Dating alluvial deposits with optically stimulated luminescence, AMS C-14 and cosmogenic techniques, western Transverse Ranges, California, USA: Quaternary Geochronology, v. 2, p. 129-136.

Doran, P. T., G. W. Berger, W. B. Lyons, J. Wharton, R. A., M. L. Davisson, J. Southon, and J. E. Dibb, 1999, Dating Quaternary lacustrine sediments in the McMurdo Dry Valleys, Antarctica: Palaeogeography, Palaeoclimatology, Palaeoecology, v. 147, p. 223-239.

Doran, P. T., McKay, C. P., Clow, G. D., Dana, G. L., Fountain, A. G., Nylen, T., and Lyons, W. B., 2002, Valley floor climate observations from the McMurdo dry valleys, Antarctica, 1986-2000: Journal of Geophysical Research-Atmospheres, v. 107, no. D24.

Duller, G. A. T., 2008, Luminescence Dating: Guidelines on using luminescence dating in archaeology: Swindon, English Hertige.

Fuchs, M., and A. Lang, 2009, Luminesescence dating of hillslope deposits- A review: Geomorphology, v. 109, p. 17-26.

Fuchs, M., and L. A. Owen, 2008, Luminescense dating of glacial and associated sediments: review, recommendations and future directions: Boreas, v. 37, p. 636-659.

Goswami, P., and J. Mishra, 2013, Climate and tectonic controls on the sedimentary processes of an alluvial fan of the Ganga Plain, India: Geology Magazine, v. 150, p. 240-253.

Hall, B. L., and G. H. Denton, 2000, Radiocarbon chronology of Ross Sea drift, eastern Taylor Valley, Antarctica: Evidence for a grounded ice sheet in the Ross Sea at the last glacial

maximum: Geografiska Annaler Series a-Physical Geography, v. 82A, no. 2-3, p. 305-336.

Hall, B. L., and G. H. Denton, 2005, Surficial geology and geomorphology of eastern and central Wright Valley, Antarctica: Geomorphology, v. 64, no. 1-2, p. 25-65.

Hall, B. L., G. H. Denton, and C. H. Hendy, 2000, Evidence from Taylor Valley for a grounded ice sheet in the Ross Sea, Antarctica: Geografiska Annaler Series a-Physical Geography, v. 82A, no. 2-3, p. 275-303.

Hambrey, M. J., and S. J. Fitzsimons, 2010, Development of sediment-landform associations at cold glacier margins, Dry Valleys, Antarctica: Sedimentology, v. 57, p. 857-882.

Harvey, A. M., P. G. Silva, A. E. Mather, J. L. Goy, M. Stokes, and C. Zazo, 1999, The impact of Quaternary sea-level and climate change on coastal alluvial fans in the Cabo de Gata ranges, southeast Spain: Geomorphology, v. 28, p. 1-22.

Harvey, A. M., 2012, The coupling status of alluvial fans and debris cones: a review and synthesis: Earth Surface Processes and Landforms, v. 37, no. 1, p. 64-76.

Haug, E. W., E. R. Kraal, J. O. Sewall, M. Van Dijk, and G. Chong Diaz, 2010, Climatic and geomorphic interactions on alluvial fans in the Atacama Desert, Chile: Geomorphology, p. 184-196.

Hendy, C. H., and Hall, B. L., 2006, The radiocarbon reservoir effect in proglacial lakes: Examples from Antarctica: Earth and Planetary Science Letters, v. 241, no. 3-4, p. 413-421.

Huybers, P., and G. Denton, 2008, Antarctic temperature at orbital timescales controlled by local summer duration: Nature Geoscience, v. 1, p. 787-792.

Huybers, P., 2009, Antarctica's Orbital Beat: Science, v. 325, no. 5944, p. 1085-1086.

Kelly, M. A., G. H. Denton, and B. L. Hall, 2002, Late Cenozoic paleoenvironment in southern Victoria Land, Antarctica, based on a polar glaciolacustrine deposit in western Victoria Valley: Geological Society of America Bulletin, v. 114, p. 605-618.

Krause, W. E., M. R. Krbetschek, and W. Stolz, 1997, Dating of Quaternary Lake sediments from the Schrimacher Oasis (East Antarctica) by Infra-red stimulated luminescence (IRSL) detected at the wavelength of 560 nm): Quaternary Science Reviews (Quaternary Geochronology), v. 1997, p. 387-392.

Lang, A., J. Moya, J. Corominas, L. Schrott, and R. Dikau, 1999, Classic and new dating methods for assessing the temporal occurrence of mass movements: Geomorphology, v. 30, p. 33-52.

Lepper, 2011, Personsal Communication. Summary of comments made during discussion period of Pardee Keynote Symposium. Geological Society of America Annual Meeting, Minneapolis, MN.

Lepper, K., N. Agersnap-Larsen, and S. W. S. McKeever, 2000, Equivalent dose distribution analysis of Holocene eolian and fluvial quartz sands from Central Oklahoma: Radiation Measurements, v. 32, p. 603-608.

Lepper, K. (2001) Development of an Objective Dose Distribution Analysis Method for OSL Dating and Pilot Studies for Planetary Applications. Dissertation, Oklahoma State University, Stillwater, OK. 288 pgs.

Lepper, K., Crowell, K, and Wilson, C. (2011) Chronology and eolian influence on colluvial apron deposition within Cañada del Buey, Pajarito Plateau, New Mexico, USA. *New Mexico Geology,* 33(1): 3-8.

Lepper, K., T. G. Fisher, I. Hajdas, and T. V. Lowell, 2007, Ages for the Big Stone Moraine and the oldest beaches of glacial Lake Agassiz: Implications for deglaciation chronology: Geology, v. 35, p. 667-670.

Lepper, K., and S. W. S. McKeever, 2002, An objective methodology for dose distribution analysis: Radiation Protection Dosimetry, v. 101, p. 349-352.

Lewis, A., and K. Lepper, unpublished. Collaborative Research: Activation of high-elevation alluvial fans in the Transantarctic Mountains – a proxy for Plio-Pleistocene warmth along East Antarctic ice margins. National Science Foundation: Division of Polar Programs. Washington, D.C., ANT-1043601.

Lian, O., and R. G. Roberts, 2006, Dating the Quaternary: progress in luminescence dating of sediments: Quaternary Science Reviews, v. 25, p. 2449-2468.

Murray, A. S., and A. G. Wintle, 2000, Luminescence dating of quartz using an improved single-aliquot regenerative-dose protocol: Radiation Measurements, v. 32, p. 57-73.

Nezat, C. A., W. B. Lyons, and K. A. Welch, 2001, Chemical weathering in streams of a polar desert (Taylor Valley, Antarctica): Geological Society of America Bulletin, v. 113, p. 1401-1408.

Parker, G., 1999, Progress in the modeling of alluvial fans: Journal of Hydraulic Research, v. 37, p. 805-825.

Prescott, J. R., and J. T. Hutton, 1988, Cosmic-ray and Gamma-ray Dosimetry for TL and Electron-spin-resonance: Nuclear Tracks and Radiation Measurements, v. 14, p. 223-227.

Prescott, J. R., and J. T. Hutton, 1994, Cosmic-ray contributions to dose-rates for luminescence and ESR dating-large depths and long-term time variations: Radiation Measurements, v. 23, p. 497-500.

Preusser, F., M. L. Chithambo, T. Gotte, M. Martini, K. Ramseyer, E. J. Sendezera, G. J. Susino, and A. G. Wintle, 2009, Quartz as a natural luminescence dosimeter: Earth-Science Reviews, v. 97, p. 184-214.

Rittenour, T. M., 2008, Luminescence dating of fluvial deposits: applications to geomorphic, palaeoseismic and archaeological research: Boreas, v. 37, p. 613-635.

Roberts, S. J., D. A. Hodgson, M. J. Bentley, D. C. W. Sanderson, G. Milne, J. A. Smith, E. Verleyen, and A. Balbo, 2009, Holocene relative sea-level change and deglaciation on Alexander Island, Antarctic Peninsula, from elevated lake deltas: Geomorphology, v. 112, p. 122-134.

Robinson, R. A. J., J. Q. G. Spencer, M. R. Strecker, A. Richter, and R. N. Alonso, 2005, Luminescence dating of alluvial fans in intramontane basins of NW Argentina, *in* A. M. Harvey, A. E. Mather, and M. Stokes, eds., Alluvial Fans: Geomorphology, Sedimentology, Dynamics: Geological Society Special Publication, v. 251, p. 153-168.

Ryder, J. M., 1971, Some aspects of the Morphometry of Paraglacial Alluvial fans in south-central British Columbia: Candian Journal of Earth Sciences, v. 8, p. 1252-1264.

Schmidt, S., S. Tsukamoto, E. Salomon, M. Frechen, and R. Hetzel, 2012, Optical dating of alluvial deposits at the orogenic front of the Andean Precordillera (Mendoza, Argentina): Geochronometria, v. 39, p. 62-75.

Simms, A. R., R. DeWitt, P. Kouremenos, and A. M. Drewry, 2011, A new approach to reconstructing sea levels in Antarctica using optically stimulated luminescence of cobble surfaces: Quaternary Geochronology, v. 6, p. 50-60.

Sohn, M. F., S. A. Mahan, J. R. Knott, and D. D. Bowman, 2007, Luminescence ages for alluvial-fan deposits in Southern Death Valley: Implications for climate-driven sedimentation along a tectonically active mountain front: Quaternary International, v. 166, p. 49-60.

Sugden, D. E., G. H. Denton, and D. R. Marchant, 1995, Landscape evolution of the Dry Valleys, Transantarctic Mountains - tectonic implications: Journal of Geophysical Research-Solid Earth, v. 100, p. 9949-9967.

Spencer, J. Q. G., and R. A. J. Robinson, 2008, Dating intramontane alluvial deposits from NW Argentina using luminescence techniques: Problems and potential: Geomorphology, v. 93, p. 144-155.

Spooner, N. A., and D. G. Questiaux, 1989, Optical dating – Achenheim beyond the Eemian using green and infrared stimulation. Long and Short Range Limits in Luminescence Dating. Occasional publication of the Research Laboratory of Archaeology and the History of Art., Oxford, p. 99-103.

Spooner, N. A., 1994, The anomalous fading of infrared-stimulated luminescence from feldspars: Radiation Measurements, v. 23, no. 2-3, p. 625-632.

Stock, J. D., K. M. Schmidt, and D. M. Miller, 2008, Controls on alluvial fan long-profiles: Geological Society of America Bulletin, v. 120, p. 619-640.

Stokes, S., 1999, Luminescence dating applications in geomorphological research: Geomorphology, v. 29, p. 153-171.

Wells, S. G., and A. M. Harvey, 1987, Sedimentologic and geomorphic variations in storm-generated alluvial fans, Howgill Fells, northwest England: Geological Society of America Bulletin, v. 98, p. 182-198.

Wintle, A. G., and A. S. Murray, 2006, A review of quartz optically stimulated luminescence characteristics and their relevance in single-aliquot regeneration dating protocols: Radiation Measurements, v. 41, p. 369-391.

Wintle, A. G., 2008, Luminescence dating: where it has been and where it is going: Boreas, v. 37, p. 471-482.

Zamora, F., 2013, Alluvial Fans in the McMurdo Dry Valleys: A proxy for melting along terrestrial margins of the East Antarctic Ice Sheet: Master's thesis.

APPENDIX. AGE CALCULATION WORKSHEETS

Sample ID FZ1102MR For samples no greater than 75 cm depth

Equivalent Dose Inputs (Gy)		De	se(De)	n	M/m
#1	Mean ± se	12.481	0.610	77/83	0.94
#2	Mode				
#3	Leading edge ± se'				
#4	recalib. Mean ± se	12.007	0.587	77/83	0.94
#5					

Dose Rate Inputs from INAA

	(ppm) ±	(ppm)	D(beta) ± (mGy/a)	(mGy/a)	D(gamma) ± (mGy/a)	(mGy/a)
K	8103	1002	0.634	0.078	0.197	0.024
Rb	39.88	9.54	0.015	0.004	---	---
Th	3.147	0.256	0.086	0.008	0.150	0.014
U	0.742	0.168	0.108	0.024	0.084	0.019

Sample Depth (cm)		5.000	
Sed./Soil Bulk Density (g/cm3)		2.000	(Aitken, 1998)
Ave. Water Content, (% ± %)		5.0	2.0
Grain Size (range; μm)		150	250
Build-up Factor		1.00	
Beta attenuation factor (BAF)		0.89	
Cosmic Dose			
Surface muon dose rate		0.220	(mGy/a)
Soft and hard component	cosmic	0.273	(mGy/a)
	(depth*density 10.000)		

Dose Rate Outputs / Effective Dose Rates (mGy/a)

	D(beta)	D(gamma)	D(cosmic)	D(totals)	
H2O correction factor	1.0625	1.057	1.057		
K	0.531	0.186	-	0.717	
Rb	0.013	-	-	0.013	
Th	0.072	0.142	-	0.214	
U	0.090	0.079	-	0.169	
Totals	0.706	0.408	0.259	**1.372**	**mGy/a**

BAF confirmed 02/23/12

Dose rate error 0.141 mGy/a

Supplemental Data Sector Fractional Dose Rates

	D(beta)	D(gamma)	D(cosmic)	D(totals)
K	0.387	0.136		0.523
Rb	0.009			0.009
U	0.052	0.104		0.156
Th	0.066	0.058		0.124
Totals	0.514	0.297	0.189	1.000

Error Analysis

	Type	#1	#2	#3	#4	#5
sigma1	ED errors	4.89	#DIV/0!	#DIV/0!	4.89	#DIV/0!
sigma2	Dose rate errors	8.87				
sigma3	Stones in matrix	0.00				
sigma4	Calibration errors	0.00				
sigma5	Parameter Uncertainties	2.97				
sigma6	U/Th uncertainty from α counting	0.00				
sigma7	Water content estimation errors	2.00				
sigma8	Uncertainty in cosmic ray dose	3.77				
	overall 1sigma error (%)	11.38	#DIV/0!	#DIV/0!	11.38	#DIV/0!

Primary Output: FZ1102MR

	De (Gy)	se[De] (Gy)	Dose Rate (mGy/a)	Dose Rate Error (mGy/a)	Age (years)	Uncert. (years)	SE of Age Distribution	Delta Method Error
#1	12.481	0.610	1.372	0.141	9098	1036	445	*1036*
#2	0.000	0.000	1.372	0.141	0		0	*0*
#3	0.000	0.000	1.372	0.141	0		0	*0*
#4	12.007	0.587	1.372	0.141	8752	996	428	*996*
#5	0.000	0.000	1.372	0.141	0		0	*0*

Sample ID FZ1105aMR **For samples no greater than 75 cm depth**

Equivalent Dose Inputs (Gy)

		De	se(De)	n	M/m
#1	Mean ± se				
#2	Fitted Mode ± se	53.184	3.624	91/95	1.15
#3	Leading edge ± se'				
#4	Recacalib. Mode ± se	51.163	3.486	91/95	1.15
#5					

Dose Rate Inputs from INAA

	(ppm) ±	(ppm)	D(beta) ± (mGy/a)	(mGy/a)	D(gamma) ± (mGy/a)	(mGy/a)
K	6640	611	0.519	0.048	0.161	0.015
Rb	45.06	11.57	0.017	0.004	---	---
Th	2.548	0.263	0.070	0.007	0.122	0.013
U	0.711	0.194	0.103	0.028	0.080	0.022

Sample Depth (cm)		20.000	
Sed./Soil Bulk Density (g/cm3)		2.000	(Aitken, 1998)
Ave. Water Content, (% ± %)		5.0	2.0
Grain Size (range; μm)		150	250
Build-up Factor		1.00	
Beta attenuation factor (BAF)		0.89	
Cosmic Dose			
Surface muon dose rate		0.220	(mGy/a)
Soft and hard component	cosmic	0.246	(mGy/a)
(depth*density	40.000)		

Dose Rate Outputs / Effective Dose Rates (mGy/a)

	D(beta)	D(gamma)	D(cosmic)	D(totals)
H2O correction factor	1.0625	1.057	1.057	
K	0.435	0.153	-	0.588
Rb	0.014	-	-	0.014
Th	0.058	0.115	-	0.173
U	0.086	0.076	-	0.162
Totals	0.594	0.344	0.233	**1.170 mGy/a**

BAF confirmed 02/23/12

Dose rate error 0.110 mGy/a

Supplemental Data Sector Fractional Dose Rates

	D(beta)	D(gamma)	D(cosmic)	D(totals)
K	0.372	0.130		0.502
Rb	0.012			0.012
U	0.050	0.098		0.148
Th	0.074	0.065		0.139
Totals	0.508	0.294	0.199	1.000

Error Analysis

	Type	#1	#2	#3	#4	#5
sigma1	ED errors	#DIV/0!	6.81	#DIV/0!	6.81	#DIV/0!
sigma2	Dose rate errors	7.71				
sigma3	Stones in matrix	0.00				
sigma4	Calibration errors	0.00				
sigma5	Parameter Uncertainties	2.93				
sigma6	U/Th uncertainty from α counting	0.00				
sigma7	Water content estimation errors	2.00				
sigma8	Uncertainty in cosmic ray dose	3.97				
	overall 1sigma error (%)	#DIV/0!	11.58	#DIV/0!	11.58	#DIV/0!

Primary Output: FZ1105aMR

	De (Gy)	se(De) (Gy)	Dose Rate (mGy/a)	Dose Rate Error (mGy/a)	Age (years)	Uncert. (years)	SE of Age Distribution	Delta Method Error
#1	0.000	0.000	1.170	0.110	0		0	*0*
#2	53.184	3.624	1.170	0.110	45453	5266	3097	*5266*
#3	0.000	0.000	1.170	0.110	0		0	*0*
#4	51.163	3.486	1.170	0.110	43725	5065	2979	*5065*
#5	0.000	0.000	1.170	0.110	0		0	*0*

Sample ID FZ1105bMR For samples no greater than 75 cm depth

Equivalent Dose Inputs (Gy)		De	se(De)	n	M/m
#1	Mean ± se				
#2	Leading edge ± se'	21.354	1.725	54/119	1.12
#3	recalib. Leading edge ± se'	20.543	1.659	54/119	1.12
#4					
#5					

Dose Rate Inputs from INAA

	(ppm) ±	(ppm)	D(beta) ± (mGy/a)	(mGy/a)	D(gamma) ± (mGy/a)	(mGy/a)
K	8922	627	0.698	0.049	0.217	0.015
Rb	38.25	5.25	0.015	0.002	---	---
Th	4.75	0.36	0.130	0.010	0.227	0.017
U	0.88	0.07	0.128	0.010	0.100	0.008

Sample Depth (cm)	40.000		
Sed./Soil Bulk Density (g/cm3)	2.000	(Aitken, 1998)	
Ave. Water Content, (% ± %)	5.0	2.0	
Grain Size (range; µm)	150	250	
Build-up Factor	1.00		
Beta attenuation factor (BAF)	0.89		
Cosmic Dose			
Surface muon dose rate	0.220	(mGy/a)	
Soft and hard component cosmic	0.219	(mGy/a)	
(depth*density 80.000)			

Dose Rate Outputs / Effective Dose Rates (mGy/a)

	D(beta)	D(gamma)	D(cosmic)	D(totals)	
H2O correction factor	1.0625	1.057	1.057		
K	0.584	0.205	-	0.790	
Rb	0.012	-	-	0.012	
Th	0.109	0.215	-	0.323	
U	0.107	0.095	-	0.202	
Totals	0.813	0.514	0.207	**1.534 mGy/a**	

BAF confirmed 02/23/12

Dose rate error 0.10 mGy/a

Supplemental Data Sector Fractional Dose Rates

	D(beta)	D(gamma)	D(cosmic)	D(totals)
K	0.381	0.134		0.515
Rb	0.008			0.008
U	0.071	0.140		0.211
Th	0.070	0.062		0.132
Totals	0.530	0.335	0.135	1.000

Error Analysis

	Type	#1	#2	#3	#4	#5
sigma1	ED errors	#DIV/0!	8.08	8.08	#DIV/0!	#DIV/0!
sigma2	Dose rate errors	4.73				
sigma3	Stones in matrix	0.00				
sigma4	Calibration errors	0.00				
sigma5	Parameter Uncertainties	3.13				
sigma6	U/Th uncertainty from α counting	0.00				
sigma7	Water content estimation errors	2.00				
sigma8	Uncertainty in cosmic ray dose	2.70				
overall 1sigma error (%)		#DIV/0!	10.43	10.43	#DIV/0!	#DIV/0!

Primary Output: FZ1105bMR

	De (Gy)	se[De] (Gy)	Dose Rate (mGy/a)	Dose Rate Error (mGy/a)	Age (years)	Uncert. (years)	SE of Age Distribution	Delta Method Error
#1	0.000	0.000	1.534	0.101	0		0	*0*
#2	21.354	1.725	1.534	0.101	13919	1452	1124	*1452*
#3	20.543	1.659	1.534	0.101	13390	1397	1082	*1397*
#4	0.000	0.000	1.534	0.101	0		0	*0*
#5	0.000	0.000	1.534	0.101	0		0	*0*

Sample ID	FZ1116bMR	For samples no greater than 75 cm depth

Equivalent Dose Inputs (Gy)

		De	se(De)	n	M/m
#1	Mean ± se				
#2	Fitted Mode ± se(ht)	9.407	0.189	64/96	1.09
#3	Leading edge ± se'	5.530	0.395	64/96	1.09
#4					
#5					

Dose Rate Inputs from INAA

	(ppm) ±	(ppm)	D(beta) ± (mGy/a)	(mGy/a)	D(gamma) ± (mGy/a)	(mGy/a)
K	6076	794	0.475	0.062	0.148	0.019
Rb	28.79	7.61	0.011	0.003	---	---
Th	3.576	0.304	0.098	0.008	0.171	0.015
U	0.944	0.157	0.137	0.023	0.107	0.018

Sample Depth (cm)	25.0		
Sed./Soil Bulk Density (g/cm3)	2.000	(Aitken, 1998)	
Ave. Water Content, (% ± %)	5.0	2.0	
Grain Size (range; µm)	150	250	
Build-up Factor	1.00		
Beta attenuation factor (BAF)	0.89		
Cosmic Dose			
Surface muon dose rate	0.220	(mGy/a)	
Soft and hard component cosmic	0.238	(mGy/a)	
(depth*density 50.000)			

Dose Rate Outputs / Effective Dose Rates (mGy/a)

	D(beta)	D(gamma)	D(cosmic)	D(totals)	
H2O correction factor	1.0625	1.057	1.057		
K	0.398	0.140	-	0.538	
Rb	0.009	-	-	0.009	
Th	0.082	0.161	-	0.243	
U	0.115	0.101	-	0.216	
Totals	0.604	0.402	0.225	**1.231**	mGy/a

BAF confirmed 02/23/12

Dose rate error 0.118 mGy/a

Supplemental Data Sector Fractional Dose Rates

	D(beta)	D(gamma)	D(cosmic)	D(totals)
K	0.323	0.113		0.437
Rb	0.007			0.007
U	0.066	0.131		0.198
Th	0.093	0.082		0.175
Totals	0.490	0.327	0.183	1.000

Error Analysis

	Type	#1	#2	#3	#4	#5
sigma1	ED errors	#DIV/0!	2.01	7.14	#DIV/0!	#DIV/0!
sigma2	Dose rate errors	8.11				
sigma3	Stones in matrix	0.00				
sigma4	Calibration errors	0.00				
sigma5	Parameter Uncertainties	2.95				
sigma6	U/Th uncertainty from α counting	0.00				
sigma7	Water content estimation errors	2.00				
sigma8	Uncertainty in cosmic ray dose	3.66				
	overall 1sigma error (%)	#DIV/0!	9.79	11.95	#DIV/0!	#DIV/0!

Primary Output: FZ1116bMR

	De (Gy)	se[De] (Gy)	Dose Rate (mGy/a)	Dose Rate Error (mGy/a)	Age (years)	Uncert. (years)	SE of Age Distribution	Delta Method Error
#1	0.000	0.000	1.231	0.118	0		0	*0*
#2	9.407	0.189	1.231	0.118	7643	749	154	*749*
#3	5.530	0.395	1.231	0.118	4493	537	321	*537*
#4	0.000	0.000	1.231	0.118	0		0	*0*
#5	0.000	0.000	1.231	0.118	0		0	*0*

Sample ID FZ1118a For samples no greater than 75 cm depth

Equivalent Dose Inputs (Gy)		De	se(De)	n	M/m
#1	Mean ± se				
#2	Fitted Mode ± se(fit)	4.585	0.176	77/143	1.52
#3	Leading edge ± se'	3.144	0.228	77/143	1.52
#4					
#5					

Dose Rate Inputs from INAA

	(ppm) ±	(ppm)	D(beta) ± (mGy/a)	(mGy/a)	D(gamma) ± (mGy/a)	(mGy/a)
K	7752	831	0.609	0.065	0.189	0.020
Rb	33.79	7.25	0.013	0.003	---	---
Th	3.447	0.294	0.094	0.008	0.164	0.014
U	1.167	0.150	0.169	0.022	0.132	0.017

Sample Depth (cm)	5.000		
Sed./Soil Bulk Density (g/cm3)	2.000	(Aitken, 1998)	
Ave. Water Content, (% ± %)	5.0	2.0	
Grain Size (range; μm)	150	250	
Build-up Factor	1.00		
Beta attenuation factor (BAF)	0.89		
Cosmic Dose			
Surface muon dose rate	0.220	(mGy/a)	
Soft and hard component cosmic	0.273	(mGy/a)	
(depth*density 10.000)			

Dose Rate Outputs / Effective Dose Rates (mGy/a)

	D(beta)	D(gamma)	D(cosmic)	D(totals)	
H2O correction factor	1.0625	1.057	1.057		
K	0.510	0.179	-	0.690	
Rb	0.011	-	-	0.011	
Th	0.079	0.156	-	0.234	
U	0.142	0.125	-	0.267	
Totals	0.742	0.459	0.259	**1.460 mGy/a**	

BAF confirmed 02/23/12

Dose rate error 0.125 mGy/a

Supplemental Data Sector Fractional Dose Rates

	D(beta)	D(gamma)	D(cosmic)	D(totals)
K	0.350	0.123		0.472
Rb	0.007			0.007
U	0.054	0.107		0.161
Th	0.097	0.085		0.183
Totals	0.508	0.315	0.177	1.000

Error Analysis

	Type	#1	#2	#3	#4	#5
sigma1	ED errors	#DIV/0!	3.84	7.25	#DIV/0!	#DIV/0!
sigma2	Dose rate errors	6.96				
sigma3	Stones in matrix	0.00				
sigma4	Calibration errors	0.00				
sigma5	Parameter Uncertainties	2.99				
sigma6	U/Th uncertainty from α counting	0.00				
sigma7	Water content estimation errors	2.00				
sigma8	Uncertainty in cosmic ray dose	3.54				
	overall 1sigma error (%)	#DIV/0!	9.41	11.25	#DIV/0!	#DIV/0!

Primary Output: FZ1118a

	De (Gy)	se(De) (Gy)	Dose Rate (mGy/a)	Dose Rate Error (mGy/a)	Age (years)	Uncert. (years)	SE of Age Distribution	Delta Method Error
#1	0.000	0.000	1.460	0.125	0		0	*0*
#2	4.585	0.176	1.460	0.125	3141	296	121	*296*
#3	3.144	0.228	1.460	0.125	2154	242	156	*242*
#4	0.000	0.000	1.460	0.125	0		0	*0*
#5	0.000	0.000	1.460	0.125	0		0	*0*

Sample ID

For samples no greater than 75 cm depth

Equivalent Dose Inputs (Gy)		De	se(De)	n	M/m
#1	Fitted Mode ± se(fit) Wb=7	56.911	2.200	93/96	1.11
#2	Leading edge ± se' Wb=7	33.385	1.883	93/96	1.11
#3	Fitted Mode ± se(fit) Wb=10	49.552	2.396	93/96	1.11
#4	Leading edge ± se' Wb=10	31.216	1.638	93/96	1.11
#5					

Dose Rate Inputs from INAA

	(ppm) ±	(ppm)	D(beta) ± (mGy/a)	(mGy/a)	D(gamma) ± (mGy/a)	(mGy/a)
K	5852	513	0.458	0.040	0.142	0.012
Rb	23.19	7.22	0.009	0.003	---	---
Th	3.321	0.294	0.091	0.008	0.158	0.014
U	1.052	0.182	0.153	0.026	0.119	0.021

Sample Depth (cm)	10.000		
Sed./Soil Bulk Density (g/cm3)	2.000	(Aitken, 1998)	
Ave. Water Content, (% ± %)	5.0	2.0	
Grain Size (range; μm)	150	250	
Build-up Factor	1.00		
Beta attenuation factor (BAF)	0.89		
Cosmic Dose			
Surface muon dose rate	0.220	(mGy/a)	
Soft and hard component cosmic	0.263	(mGy/a)	
(depth*density 20.000)			

Dose Rate Outputs / Effective Dose Rates (mGy/a)

	D(beta)	D(gamma)	D(cosmic)	D(totals)	
H2O correction factor	1.0625	1.057	1.057		
K	0.383	0.135	-	0.518	
Rb	0.007	-	-	0.007	
Th	0.076	0.150	-	0.226	
U	0.128	0.112	-	0.240	
Totals	0.594	0.397	0.249	**1.241** mGy/a	

BAF confirmed 02/23/12

Dose rate error 0.105 mGy/a

Supplemental Data Sector Fractional Dose Rates

	D(beta)	D(gamma)	D(cosmic)	D(totals)
K	0.309	0.108		0.417
Rb	0.006			0.006
U	0.061	0.121		0.182
Th	0.103	0.091		0.194
Totals	0.479	0.320	0.201	1.000

Error Analysis

	Type	#1	#2	#3	#4	#5
sigma1	ED errors	3.87	5.64	4.84	5.25	#DIV/0!
sigma2	Dose rate errors	6.53				
sigma3	Stones in matrix	0.00				
sigma4	Calibration errors	0.00				
sigma5	Parameter Uncertainties	2.88				
sigma6	U/Th uncertainty from α counting	0.00				
sigma7	Water content estimation errors	2.00				
sigma8	Uncertainty in cosmic ray dose	4.02				
	overall 1sigma error (%)	9.28	10.15	9.72	9.93	#DIV/0!

Primary Output: 0

	De (Gy)	se(De) (Gy)	Dose Rate (mGy/a)	Dose Rate Error (mGy/a)	Age (years)	Uncert. (years)	SE of Age Distribution	Delta Method Error
#1	56.911	2.200	1.241	0.105	45876	4256	1773	*4256*
#2	33.385	1.883	1.241	0.105	26912	2730	1518	*2730*
#3	49.552	2.396	1.241	0.105	39944	3883	1931	*3883*
#4	31.216	1.638	1.241	0.105	25163	2499	1320	*2499*
#5	0.000	0.000	1.241	0.105	0		0	*0*

Sample ID	FZ1118cMR	For samples no greater than 75 cm depth

Equivalent Dose Inputs (Gy)

		De	se(De)	n	M/m
#1	Mean ± se				
#2	Fitted Mode ± se(fit)	266.219	23.634	24/142	1.17
#3	Leading edge ± se'	82.769	32.168	24/142	1.17
#4	recalb. Leading edge	79.624	30.946	24/142	1.17
#5					

Dose Rate Inputs from INAA

	(ppm) ±	(ppm)	D(beta) ± (mGy/a)	(mGy/a)	D(gamma) ± (mGy/a)	(mGy/a)
K	7467	806	0.584	0.063	0.181	0.020
Rb	40.49	7.62	0.015	0.003	---	---
Th	3.992	0.328	0.109	0.009	0.190	0.016
U	1.025	0.143	0.149	0.021	0.116	0.016

Sample Depth (cm)		25.000	
Sed./Soil Bulk Density (g/cm3)		2.000	(Aitken, 1998)
Ave. Water Content, (% ± %)		5.0	2.0
Grain Size (range; µm)		150	250
Build-up Factor		1.00	
Beta attenuation factor (BAF)		0.89	
Cosmic Dose			
Surface muon dose rate		0.220	(mGy/a)
Soft and hard component	cosmic	0.238	(mGy/a)
(depth*density	50.000)		

Dose Rate Outputs / Effective Dose Rates (mGy/a)

	D(beta)	D(gamma)	D(cosmic)	D(totals)	
H2O correction factor	1.0625	1.057	1.057		
K	0.489	0.172	-	0.661	
Rb	0.013	-	-	0.013	
Th	0.091	0.180	-	0.271	
U	0.124	0.110	-	0.234	
Totals	0.718	0.461	0.225	1.404	mGy/a

BAF confirmed 02/23/12

Dose rate error 0.119 mGy/a

Supplemental Data Sector Fractional Dose Rates

	D(beta)	D(gamma)	D(cosmic)	D(totals)
K	0.348	0.122		0.471
Rb	0.009			0.009
U	0.065	0.128		0.193
Th	0.089	0.078		0.167
Totals	0.511	0.329	0.160	1.000

Error Analysis

	Type	#1	#2	#3	#4	#5
sigma1	ED errors	#DIV/0!	8.88	38.86	38.87	#DIV/0!
sigma2	Dose rate errors	6.92				
sigma3	Stones in matrix	0.00				
sigma4	Calibration errors	0.00				
sigma5	Parameter Uncertainties	3.04				
sigma6	U/Th uncertainty from α counting	0.00				
sigma7	Water content estimation errors	2.00				
sigma8	Uncertainty in cosmic ray dose	3.21				
	overall 1sigma error (%)	#DIV/0!	12.26	39.77	39.77	#DIV/0!

Primary Output: FZ1118cMR

	De (Gy)	se(De) (Gy)	Dose Rate (mGy/a)	Dose Rate Error (mGy/a)	Age (years)	Uncert. (years)	SE of Age Distribution	Delta Method Error
#1	0.000	0.000	1.404	0.119	0		0	*0*
#2	266.219	23.634	1.404	0.119	189562	23232	16829	*23232*
#3	82.769	32.168	1.404	0.119	58936	23440	22905	*23440*
#4	79.624	30.946	1.404	0.119	56696	22550	22035	*22550*
#5	0.000	0.000	1.404	0.119	0		0	*0*

Sample ID FZ1118eMR For samples no greater than 75 cm depth

Equivalent Dose Inputs (Gy)		De	se(De)	n	M/m
#1	Mean ± se				
#2	Fitted Mode ± se(fit)	139.457	13.428	29/118	1.15
#3	Leading edge ± se'	79.995	9.793	29/118	1.15
#4	Recalib. Fitted Mode	134.158	12.918	29/118	1.15
#5					

Dose Rate Inputs from INAA

	(ppm) ±	(ppm)	D(beta) ± (mGy/a)	(mGy/a)	D(gamma) ± (mGy/a)	(mGy/a)
K	6322	583	0.494	0.046	0.154	0.014
Rb	38.07	8.69	0.014	0.003	---	---
Th	3.367	0.294	0.092	0.008	0.161	0.014
U	1.113	0.174	0.161	0.025	0.126	0.020

Sample Depth (cm)	35.000		
Sed./Soil Bulk Density (g/cm3)	2.000	(Aitken, 1998)	
Ave. Water Content, (% ± %)	5.0	2.0	
Grain Size (range; µm)	150	250	
Build-up Factor	1.00		
Beta attenuation factor (BAF)	0.89		
Cosmic Dose			
Surface muon dose rate	0.220	(mGy/a)	
Soft and hard component cosmic	0.225	(mGy/a)	
(depth*density 70.000)			

Dose Rate Outputs / Effective Dose Rates (mGy/a)

	D(beta)	D(gamma)	D(cosmic)	D(totals)	
H2O correction factor	1.0625	1.057	1.057		
K	0.414	0.145	-	0.559	
Rb	0.012	-	-	0.012	
Th	0.077	0.152	-	0.229	
U	0.135	0.119	-	0.254	
Totals	0.638	0.416	0.213	**1.267** mGy/a	

BAF confirmed 02/23/12

Dose rate error 0.103 mGy/a

Supplemental Data: Sector Fractional Dose Rates

	D(beta)	D(gamma)	D(cosmic)	D(totals)
K	0.327	0.115		0.441
Rb	0.010			0.010
U	0.061	0.120		0.181
Th	0.107	0.094		0.201
Totals	0.504	0.328	0.168	1.000

Error Analysis

	Type	#1	#2	#3	#4	#5
sigma1	ED errors	#DIV/0!	9.63	12.24	9.63	#DIV/0!
sigma2	Dose rate errors	6.46				
sigma3	Stones in matrix	0.00				
sigma4	Calibration errors	0.00				
sigma5	Parameter Uncertainties	3.01				
sigma6	U/Th uncertainty from α counting	0.00				
sigma7	Water content estimation errors	2.00				
sigma8	Uncertainty in cosmic ray dose	3.36				
	overall 1sigma error (%)	#DIV/0!	12.60	14.70	12.60	#DIV/0!

Primary Output: FZ1118eMR

	De (Gy)	se(De) (Gy)	Dose Rate (mGy/a)	Dose Rate Error (mGy/a)	Age (years)	Uncert. (years)	SE of Age Distribution	Delta Method Error
#1	0.000	0.000	1.267	0.103	0		0	*0*
#2	139.457	13.428	1.267	0.103	110043	13867	10596	*13867*
#3	79.995	9.793	1.267	0.103	63122	9276	7727	*9276*
#4	134.158	12.918	1.267	0.103	105861	13340	10193	*13340*
#5	0.000	0.000	1.267	0.103	0		0	*0*

Sample ID FZ1126b For samples no greater than 75 cm depth

Equivalent Dose Inputs (Gy)		De	se(De)	n	M/m
#1	Mean ± se				
#2	Fitted Mode ± se(fit)	15.875	0.483	86/96	1.63
#3	Leading edge ± se'	7.475	1.186	86/96	1.63
#4	Recalib. Leading Edge	7.191	1.141	86/96	1.63
#5					

Dose Rate Inputs from INAA

	(ppm) ±	(ppm)	D(beta) ± (mGy/a)	(mGy/a)	D(gamma) ± (mGy/a)	(mGy/a)
K	8080	981	0.632	0.077	0.196	0.024
Rb	30.25	10.21	0.011	0.004	---	---
Th	4.561	0.380	0.125	0.010	0.218	0.018
U	1.444	0.212	0.209	0.031	0.163	0.024

Sample Depth (cm)	25.000		
Sed./Soil Bulk Density (g/cm3)	2.000	(Aitken, 1998)	
Ave. Water Content, (% ± %)	5.0	2.0	
Grain Size (range; µm)	150	250	
Build-up Factor	1.00		
Beta attenuation factor (BAF)	0.89		
Cosmic Dose			
Surface muon dose rate	0.220	(mGy/a)	
Soft and hard component cosmic	0.238	(mGy/a)	
(depth*density 50.000)			

Dose Rate Outputs / Effective Dose Rates (mGy/a)

	D(beta)	D(gamma)	D(cosmic)	D(totals)
H2O correction factor	1.0625	1.057	1.057	
K	0.529	0.186	-	0.715
Rb	0.010	-	-	0.010
Th	0.104	0.206	-	0.310
U	0.175	0.154	-	0.330
Totals	0.819	0.546	0.225	**1.590 mGy/a**

BAF confirmed 02/23/12

Dose rate error 0.141 mGy/a

Supplemental Data Sector Fractional Dose Rates

	D(beta)	D(gamma)	D(cosmic)	D(totals)
K	0.333	0.117		0.450
Rb	0.006			0.006
U	0.066	0.129		0.195
Th	0.110	0.097		0.207
Totals	0.515	0.343	0.142	1.000

Error Analysis

	Type	#1	#2	#3	#4	#5
sigma1	ED errors	#DIV/0!	3.04	15.87	15.87	#DIV/0!
sigma2	Dose rate errors	7.53				
sigma3	Stones in matrix	0.00				
sigma4	Calibaration errors	0.00				
sigma5	Parameter Uncertainties	3.09				
sigma6	U/Th uncertainty from α counting	0.00				
sigma7	Water content estimation errors	2.00				
sigma8	Uncertainty in cosmic ray dose	2.83				
	overall 1sigma error (%)	#DIV/0!	9.36	18.17	18.17	#DIV/0!

Primary Output: FZ1126b

	De (Gy)	se(De) (Gy)	Dose Rate (mGy/a)	Dose Rate Error (mGy/a)	Age (years)	Uncert. (years)	SE of Age Distribution	Delta Method Error
#1	0.000	0.000	1.590	0.141	0		0	*0*
#2	15.875	0.483	1.590	0.141	9986	934	304	*934*
#3	7.475	1.186	1.590	0.141	4702	854	746	*854*
#4	7.191	1.141	1.590	0.141	4523	822	718	*822*
#5	0.000	0.000	1.590	0.141	0		0	*0*

Sample ID FZ1150aMR For samples no greater than 75 cm depth

Equivalent Dose Inputs (Gy)		De	se(De)	n	M/m
#1	Mean ± se	38.176	4.883	27/119	1.23
#2	Fitted Mode ± se(fit)	27.265	0.957	27/119	1.23
#3	Leading edge ± se'	12.185	1.031	27/119	1.23
#4	Recalib. Fitted Mode	26.229	0.921	27/119	1.23
#5					

Dose Rate Inputs from INAA

	(ppm) ±	(ppm)	D(beta) ± (mGy/a)	(mGy/a)	D(gamma) ± (mGy/a)	(mGy/a)
K	16631	1252	1.301	0.098	0.404	0.030
Rb	91.20	11.35	0.035	0.004	---	---
Th	5.90	0.47	0.161	0.013	0.281	0.023
U	0.90	0.26	0.130	0.038	0.101	0.030

Sample Depth (cm)	5.000		
Sed./Soil Bulk Density (g/cm3)	2.000	(Aitken, 1998)	
Ave. Water Content, (% ± %)	5.0	2.0	
Grain Size (range; µm)	150	250	
Build-up Factor	1.00		
Beta attenuation factor (BAF)	0.89		
Cosmic Dose			
Surface muon dose rate	0.220	(mGy/a)	
Soft and hard component cosmic	0.273	(mGy/a)	
(depth*density 10.000)			

Dose Rate Outputs / Effective Dose Rates (mGy/a)

	D(beta)	D(gamma)	D(cosmic)	D(totals)
H2O correction factor	1.0625	1.057	1.057	
K	1.089	0.382	-	1.472
Rb	0.029	-	-	0.029
Th	0.135	0.266	-	0.401
U	0.109	0.096	-	0.205
Totals	1.362	0.744	0.259	**2.365 mGy/a**

BAF confirmed 02/23/12

Dose rate error 0.180 mGy/a

Supplemental Data Sector Fractional Dose Rates

	D(beta)	D(gamma)	D(cosmic)	D(totals)
K	0.461	0.162		0.622
Rb	0.012			0.012
U	0.057	0.112		0.169
Th	0.046	0.041		0.087
Totals	0.576	0.315	0.109	1.000

Error Analysis

	Type	#1	#2	#3	#4	#5
sigma1	ED errors	12.79	3.51	8.46	3.51	#DIV/0!
sigma2	Dose rate errors	6.17				
sigma3	Stones in matrix	0.00				
sigma4	Calibration errors	0.00				
sigma5	Parameter Uncertainties	3.28				
sigma6	U/Th uncertainty from α counting	0.00				
sigma7	Water content estimation errors	2.00				
sigma8	Uncertainty in cosmic ray dose	2.19				
	overall 1sigma error (%)	14.87	8.36	11.37	8.36	#DIV/0!

Primary Output: FZ1150aMR

	De (Gy)	se(De) (Gy)	Dose Rate (mGy/a)	Dose Rate Error (mGy/a)	Age (years)	Uncert. (years)	SE of Age Distribution	Delta Method Error
#1	38.176	4.883	2.365	0.180	16142	2401	2065	*2401*
#2	27.265	0.957	2.365	0.180	11528	964	405	*964*
#3	12.185	1.031	2.365	0.180	5152	586	436	*586*
#4	26.229	0.921	2.365	0.180	11090	928	389	*928*
#5	0.000	0.000	2.365	0.180	0		0	*0*

Sample ID FZ1152aMR For samples no greater than 75 cm depth

Equivalent Dose Inputs (Gy)		De	se(De)	n	M/m
#1	Mean ± se	23.624	3.302	57/118	1.53
#2	Fitted Mode ± se(fit)	13.537	0.185	57/118	1.53
#3	Leading edge ± se'	7.441	1.217	57/118	1.53
#4	Recalib. Fitted Mode	13.023	0.178	57/118	1.53
#5					

Dose Rate Inputs from INAA

	(ppm) ±	(ppm)	D(beta) ± (mGy/a)	(mGy/a)	D(gamma) ± (mGy/a)	(mGy/a)
K	8876	822	0.694	0.064	0.216	0.020
Rb	42.63	11.53	0.016	0.004	---	---
Th	2.81	0.27	0.077	0.007	0.134	0.013
U	0.86	0.30	0.125	0.044	0.097	0.034

Sample Depth (cm)	5.000		
Sed./Soil Bulk Density (g/cm3)	2.000	(Aitken, 1998)	
Ave. Water Content, (% ± %)	5.0	2.0	
Grain Size (range; μm)	150	250	
Build-up Factor	1.00		
Beta attenuation factor (BAF)	0.89		
Cosmic Dose			
Surface muon dose rate	0.220	(mGy/a)	
Soft and hard component cosmic	0.273	(mGy/a)	
(depth*density 10.000)			

Dose Rate Outputs / Effective Dose Rates (mGy/a)

	D(beta)	D(gamma)	D(cosmic)	D(totals)
H2O correction factor	1.0625	1.057	1.057	
K	0.581	0.204	-	0.785
Rb	0.014	-	-	0.014
Th	0.064	0.127	-	0.191
U	0.105	0.092	-	0.197
Totals	0.764	0.423	0.259	1.446 mGy/a

BAF confirmed 02/23/12

Dose rate error 0.145 mGy/a

Supplemental Data Sector Fractional Dose Rates

	D(beta)	D(gamma)	D(cosmic)	D(totals)
K	0.402	0.141		0.543
Rb	0.009			0.009
U	0.044	0.088		0.132
Th	0.072	0.064		0.136
Totals	0.528	0.293	0.179	1.000

Error Analysis

	Type	#1	#2	#3	#4	#5
sigma1	ED errors	13.98	1.37	16.36	1.37	#DIV/0!
sigma2	Dose rate errors	8.60				
sigma3	Stones in matrix	0.00				
sigma4	Calibaration errors	0.00				
sigma5	Parameter Uncertainties	3.02				
sigma6	U/Th uncertainty from α counting	0.00				
sigma7	Water content estimation errors	2.00				
sigma8	Uncertainty in cosmic ray dose	3.58				
overall 1sigma error (%)		17.18	10.09	19.17	10.09	#DIV/0!

Primary Output: FZ1152aMR

	De (Gy)	se(De) (Gy)	Dose Rate (mGy/a)	Dose Rate Error (mGy/a)	Age (years)	Uncert. (years)	SE of Age Distribution	Delta Method Error
#1	23.624	3.302	1.446	0.145	16342	2808	2284	*2808*
#2	13.537	0.185	1.446	0.145	9364	945	128	*945*
#3	7.441	1.217	1.446	0.145	5147	987	842	*987*
#4	13.023	0.178	1.446	0.145	9009	909	123	*909*
#5	0.000	0.000	1.446	0.145	0		0	*0*